MECA0023-A-a Advanced solid mechanics

Project

Cube subjected to surface traction

Adam Caroline (s172593)
Atceken Seyda-Nur (s176145)
Jeholet Chloé (s172146)
Lahaye Lucile (s171341)

Professor : Ponthot J.-P.
Teaching Assistant : Laruelle C.

Section : Master in aerospace engineering
Group 1

Liege University
School of Engineering

Academic Year 2020-2021

Contents

List of Figures

Introduction

In solid mechanics, it is essential to be able to build a mathematical model reproducing the experimental 3D observations. To achieve this, the understanding of the plastic, visco-plastic and visco-elastic behaviors of the material is primordial.

The aim of this study is to analyze in depth the evolution of the stresses and strains in a cube undergoing uni-axial surface traction and compression. The investigation is realized using Metafore, a non-linear finite element software allowing the calculation of structures in the elasto-plastic domain.

The analysis is divided into four main parts. The first one aims to deal with elasto-plastic materials combined with linear hardening models such as the isotropic, the kinematic and the mixed ones. Both plane stress and plane strain states will be presented in this first study. Then, the analysis will be extended for non-linear hardening behaviors in the second part, for the plane stress state only. A third part will introduce the viscosity parameter and its influence on the previous results in the case of linear hardening models. Finally, in the fourth part, the sensitivity of the previous numerical analyses to the different parameters as the time step or the mesh will be investigated.

In this project, both analytical and numerical results will be compared for different variables such as the yield stress, the equivalent visco-plastic strain or the equivalent stress.

Definition of the material

Several hypothesis are made in order to simplify the study. Indeed, the inertial forces and the temperature effects are neglected to obtain an isothermal problem with a quasi-static loading. In addition to this, the material is assumed to be a J_2-Von Mises material. This means that the Von Mises yield criterion is only based on the J_2 invariant so that the yield function is even. Finally, the hypothesis of small strains is made in the whole project.

The specific properties of the material are given here below:

$$\begin{cases} \rho = 7850 \text{ kg/m}^3 \\ E = 205000 \text{ MPa} \\ \nu = 0.3 \\ h = 30000 \text{ MPa} \\ \theta = \theta^* = 0.2 \\ \bar{\varepsilon}^{vp}_{\max} = 0.25\% \\ \sigma^0_y = 200 \text{ MPa} \\ \sigma^\infty_y = 300 \text{ MPa} \\ A = S^2 = 10000 \text{ mm}^2 \end{cases} \tag{1}$$

Definition of the loading

In this project, the loading corresponds to a surface traction (positive or negative) $\sigma_{11}(t)$, the stress will thus be directed in the $\boldsymbol{e}_1$ direction. This traction will be applied on the

upper surface of the cube and the displacement due to this force will be studied only at the point number 7 (cf. Fig. 1).

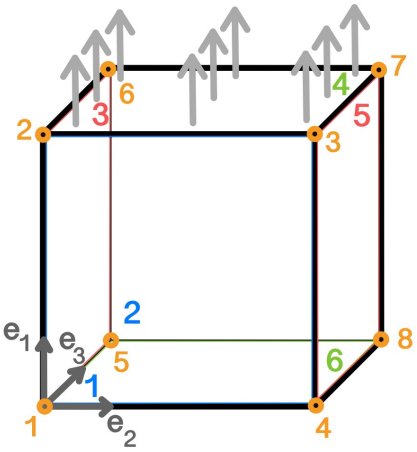

Figure 1: Geometry of the cube studied.

The load that will start from 0 will be increased linearly to the maximal load $t_{\max}$, then it will be decreased linearly until $-t_{\max}$ and will be finally brought back to zero, defining a sawtooth path. This value $t_{\max}$ is computed in Section 1.2 for a linear isotropic hardening law. This loading/unloading cycle will last 10s and will be repeated three times in most of the study to clearly see the evolution of the interesting variables over time. The cube will thus undergo tensile and compressive stresses alternatively (cf. Fig 2).

It must be taken into account that the applied load depends on time even if it will not always be specified in the following report.

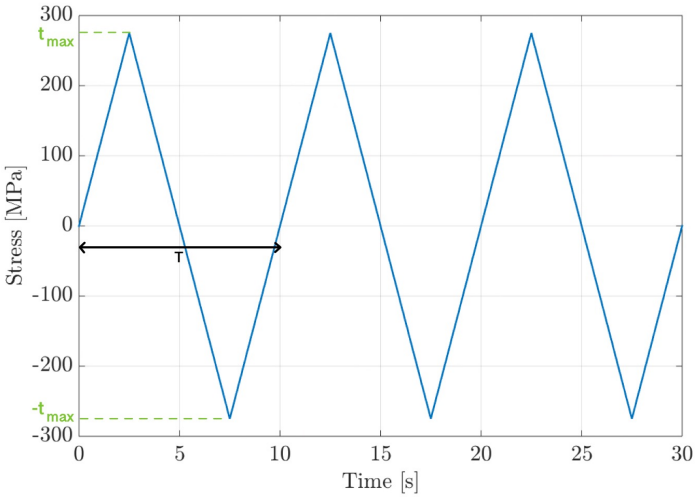

Figure 2: Loading/unloading cycles.

Definition of the mesh

The cube is only submitted to an uni-axial surface traction so the strains and the stresses are uniform inside this one. Therefore, a mesh composed of one single element is enough

to get accurate results for this type of numerical simulations.

Moreover, the displacements computed during this project are only considered at one point of the cube (the point number 7) so, the meshing of the cube has no consequence on the results measured.

To conclude, the whole study will be done with only one element of mesh.

Definition of the plastic variables

The plasticity can be described thanks to the definition of several internal variables.

First, the yield stress σ_y is the stress at which the plasticity begins. It is always equal to σ_y^0 for the virgin material, then its evolution to the subsequent yield stress depends on the considered hardening model. The radius of Von Mises current yield surface corresponds to $\sqrt{2/3}\,\sigma_y$.

A second essential parameter is the effective plastic strain $\bar{\varepsilon}^p$, a quantity that will never decrease during plasticity, even in compression. Indeed, its definition is based on the integral of the effective plastic strain rate:

$$\bar{\varepsilon}^{vp}(t) = \bar{\varepsilon}^p(t_0) + \int_{t_0}^{t} \dot{\bar{\varepsilon}}^{vp}(\tau)\,\mathrm{d}\tau = \bar{\varepsilon}^p(t_0) + \int_{t_0}^{t} \sqrt{\frac{2}{3} D_{ij}^{vp} D_{ij}^{vp}}\,\mathrm{d}\tau, \tag{2}$$

where $\mathbf{D}^{vp}$ is the visco-plastic deformation strain rate. For small displacements, $D_{ij}^{vp} = \dot{\varepsilon}_{ij}^{vp}$.

Another internal variable that plays an important role is the backstress tensor $\boldsymbol{\alpha}$ that represents the current center of the yield surface. This parameter depends strongly on the hardening laws considered and it will thus be described in each different sections.

Part I

Elasto-plastic behavior with linear hardening

In this first part, the behavior of elasto-plastic materials with linear hardening laws are analyzed. The isotropic, kinematic and mixed hardening laws are studied in the different sections for a plane stress configuration and then for a plane strain state.

1 Plane stress state

In the first configuration, the traction $\sigma_{11}(t)$ is applied only on one face (the upper surface of the cube) while the displacements are only blocked in a corner of the cube: the face 1 is blocked along $\mathbf{e}_3$, the face 3 along $\mathbf{e}_2$ and the face 6 along $\mathbf{e}_1$ (cf. colored faces Fig. 3). In this state, the cube is free to deform along $\mathbf{e}_1$,$\mathbf{e}_2$ and $\mathbf{e}_3$. With these boundary conditions, when a loading $\sigma_{11}(t)$ is applied, the cube undergoes traction or compression along the first direction and due to the Poisson's effect, the cube deforms also in the other two directions.

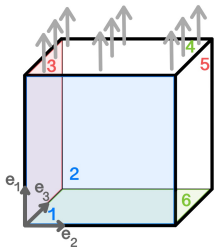

Figure 3: Plane stress state.

The problem corresponds therefore to a uni-axial loading where the stress and strain tensors can be written as:

$$\boldsymbol{\sigma}(t) = \begin{pmatrix} \sigma_{11}(t) & 0 & 0 \\ 0 & 0 & 0 \\ 0 & 0 & 0 \end{pmatrix} \quad \text{and} \quad \boldsymbol{\varepsilon}(t) = \begin{pmatrix} \varepsilon_{11}(t) & 0 & 0 \\ 0 & \varepsilon_{22}(t) & 0 \\ 0 & 0 & \varepsilon_{33}(t) \end{pmatrix}. \tag{3}$$

For the cube in plane stress state, the stress deviatoric $\boldsymbol{s}$ tensor can also be computed:

$$\boldsymbol{s} = \text{dev}(\boldsymbol{\sigma}) \; = \; \boldsymbol{\sigma} - \frac{1}{3}\,\text{tr}(\boldsymbol{\sigma}) \tag{4}$$

$$\Leftrightarrow \boldsymbol{s}(t) = \begin{pmatrix} \frac{2}{3}\sigma_{11}(t) & 0 & 0 \\ 0 & -\frac{1}{3}\sigma_{11}(t) & 0 \\ 0 & 0 & -\frac{1}{3}\sigma_{11}(t) \end{pmatrix}. \tag{5}$$

Thanks to this, the stress deviator invariant J_2 can be computed from its definition:

$$J_2 = \frac{1}{2}s_{ij}s_{ij} = \frac{1}{2}\sigma_{11}^2(t)(\frac{4}{9} + \frac{1}{9} + \frac{1}{9}) = \frac{1}{3}\sigma_{11}^2(t). \tag{6}$$

For the following developments, it is interesting to notice that, thanks to the definition of J_2, $\sqrt{\frac{3}{2}s_{ij}s_{ij}} = \sqrt{3J_2}$ is the absolute value of the applied stress $|\sigma_{11}(t)|$. Thus, when

the applied load will take a zero value while its evolution between $t_{\max}$ and $-t_{\max}$, the value of $\sqrt{3J_2}$ will be equal to zero too.

1.1 Perfectly plastic model

When there is no hardening at all, the material is known as a perfectly plastic solid. In this case, the plastic slope E_T is zero and thus the isotropic hardening coefficient $h = \frac{EE_T}{E-E_T}$ is zero too. The yield criterion can be written, in the case of a J_2 Von-Mises material, as:

$$f = \sqrt{\frac{3}{2}s_{ij}s_{ij}} - \sigma_y^0 = \sqrt{3J_2} - \sigma_y^0 = \bar{\sigma} - \sigma_y^0 \leq 0, \tag{7}$$

where $\sigma_y^0 = 200$ MPa is the constant virgin yield stress and $\bar{\sigma}$ the equivalent stress.

In this section of plane stress state, since the load only has a component in the first principal direction, the stress state will evolve only in this direction. Thus, the study in the *Haigh Westergaard's space* will always be brought in two dimensions (in the plane $\sigma_1 - \sigma_2$) for more simplicity.

The yield surface of Eq. 7 can be represented in the *Haigh Westergaard's space* as on the left of Fig. 4. This shows that for $\bar{\sigma} < \sigma_y^0$, the regime is purely elastic. And once σ_y^0 is reached, the material can keep deforming without increasing the applied stress or it can be unloaded elastically and go back inside the surface. Because there is no hardening, the yield surface does not evolve with the stress history.

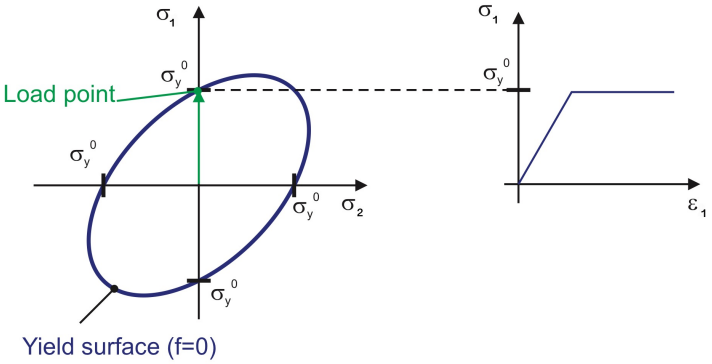

Figure 4: Perfectly plastic case: *Haigh Westergaard's space* curve and stress-strain curve.

Using Metafor to test this perfectly plastic case, a problem is encountered while applying a traction of 200 MPa or more : the software stops compiling and returns an error message. For a stress of 200 MPa, an infinite number of corresponding strain exists and above that value, it is the forbidden region for which $f > 0$. Metafor is thus not able to represent this kind of stress driven problem.

1.2 Linear isotropic hardening

Since the previous law is not able to represent the reality of most metals that harden while being plastically deformed, an isotropic hardening law is introduced. In this case, the elastic domain is increased but remains always symmetric about $\sigma = 0$. The subsequent yield stress depends therefore on the loading history of the material, thus on the effective

plastic strain $\bar{\varepsilon}^p$ and grows as:

$$\sigma_y(\bar{\varepsilon}^p) = \sigma_y^0 + h_i(\bar{\varepsilon}^p)\bar{\varepsilon}^p. \tag{8}$$

For a linear hardening, $h_i(\bar{\varepsilon}^p) = h_i = h$ is constant.

Similarly, in the *Haigh Westergaard's space*, the yield surface is expanding in size uniformly in all directions of the stress space when the material hardens. The expression of the yield function in the case of a J_2Von-Mises material is therefore:

$$f = \sqrt{\frac{3}{2}s_{ij}s_{ij}} - \sigma_y(\bar{\varepsilon}^p) = \sqrt{3J_2} - \sigma_y(\bar{\varepsilon}^p) = \bar{\sigma} - \sigma_y(\bar{\varepsilon}^p) \leq 0. \tag{9}$$

In order to define the loading cycle, the maximum surface traction $t_{\max}$ needed to reach a permanent equivalent plastic deformation must be computed for particular material data as those mentioned in System (1).

Using Eq. 8, the maximum stress can be computed:

$$t_{\max} = \sigma_y^{\max}(\bar{\varepsilon}^p) = \sigma_y^0 + h\bar{\varepsilon}^{vp}_{\max} = 200 + 30000 \times 0.0025 = 275 \text{ MPa}. \tag{10}$$

It is important to note that this value will be the maximum one applied on the cube for all the loading and unloading next cycles of the different parts if not mentioned.

Some interesting variables can now be analyzed in order to understand this model when applying the sawtooth loading. Different times of the first period have been retained to observe all the important states of the loading/unloading process: between 0 and 1.8s it is the elastic loading, between 1.8s and 2.5s the hardening , at 2.5s the maximum load in tension and then the unload and the reload in compression.

One can note that, as there is no backstress in an isotropic hardening case, the Von-Mises effective stress $\bar{\sigma}^{VM}$ is equal to the equivalent stress $\bar{\sigma} = \sqrt{3J_2}$. As it can be seen on Fig. 5a, it corresponds so to the absolute value of the applied stress $\sigma_{11}(t)$.

In a first time, the applied force is increased linearly from 0 to $t_{\max}$. So at 1s for example, the equivalent stress $\bar{\sigma}$ is lower than σ_y^0 (cf. Fig. 5a). It means that the loading is still in the elastic domain. The equivalent plastic strain $\bar{\varepsilon}^p$ is thus zero (cf. Fig. 5b) and in the *Haigh Westergaard's space*, the state is inside the yield surface (blue point inside the blue ellipse Fig. 6a).

At 1.8s, $\bar{\sigma}$ reaches $\sigma_y^0 = 200MPa$. One can notice than the strain in the $\boldsymbol{e_1}$ direction ε_{11} firstly evolves with a certain slope but after this point, the slope is abruptly increased (cf. Fig. 5b). This corresponds in fact to the entry in plasticity of the material. Because of the Poisson's effect, the strains in the two others direction are non-zero: $\varepsilon_{22} = \varepsilon_{33} = -\nu\varepsilon_{11}$. As the load keeps growing, the material is then hardened which corresponds to an expansion of the yield surface. As an example, the orange ellipse (Fig. 6a) is the expanded yield surface at time $t = 2s$. This one expands until the applied stress reaches the maximum stress $t_{\max}$ at 2.5s (the yellow ellipse). During this laps of time, the yield stress and the equivalent plastic strain are increased to their maximal values (cf. Fig. 5a and 5b).

Between 2.5s and 5s the cube is unloaded. We are now inside the yield surface so in

the elastic domain. Between 5s and 10s the cube is loaded and unloaded in a similar way but in compression and not in traction anymore. Because the applied load will never be larger than the maximum stress $t_{\max}$, the material will never be hardened anymore and the subsequent yield stress and the equivalent plastic strain will always stay constant. On the stress-strain space (cf. Fig. 6b), it thus means that the state will travel between the yellow point and the purple point in a purely elastic regime. A permanent plastic deformation is observed.

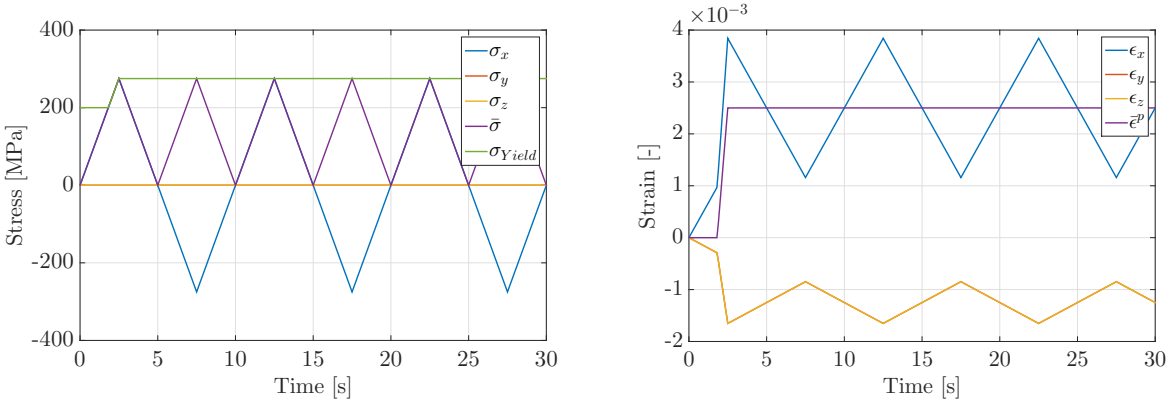

(a) Evolution in time of the stresses.

(b) Evolution in time of the strains.

Figure 5: Linear isotropic hardening in a plane stress state.

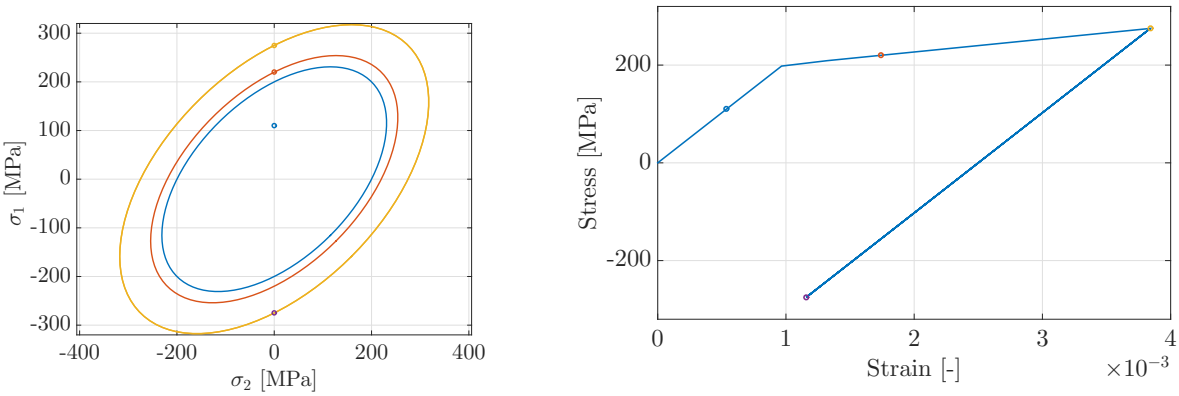

(a) Westergaard's space.

(b) Stress-strain space.

Figure 6: Linear isotropic hardening in a plane stress state
blue dot = 1s, orange dot = 2s, yellow dot = 2.5s, purple dot = 7.5s.

1.3 Linear kinematic hardening

There exists also another way to describe the hardening of the material: the kinematic hardening. In this part, only the linear hardening will be studied (cf. Part II for non-linear investigations).

The main reason of introducing this new law is to make up for a weak point of the isotropic hardening law: its incapacity to represent *Bauschinger effect*. In the kinematic hardening model, the evolution of the yield surface during plasticity consists in its translation without any modification of its size. The position of the center of the yield surface is defined by the backstress tensor $\boldsymbol{\alpha}$.

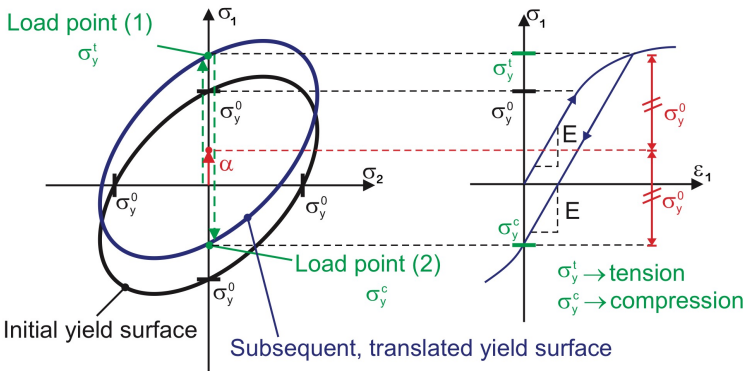

Figure 7: Kinematic hardening.

As it can be seen in Fig. 7, the elastic domain has a constant size of $2 \times \sigma_y^0$ and the translation of its center by α leads to the fact that the yield stress in reverse direction is substantially slower than the yield stress in the original direction. The *Bauschinger effect* can therefore be taken into account in this model.

The law used to describe the linear evolution of the backstress is the one proposed by *Melan and Prager*:

$$\dot{\alpha}_{ij} = \frac{2}{3} h_k D^p_{ij}, \tag{11}$$

where $h_k = h$ [MPa] and D^p_{ij} are the plastic strain rate tensor components.

Thanks to *Bridgman experiments*, it is known that the pressure does not influence the plasticity, so that $\mathbf{D}^p$ is deviatoric, and so $\dot{\alpha}$ and α too by Eq. 11. Since there is no shear in this problem, $\boldsymbol{\alpha}$ is a diagonal tensor. Using the fact that the stress is applied in $\mathbf{e}_1$ direction and considering isotropic conditions in the other two directions, the backstress tensor has the form:

$$\boldsymbol{\alpha} = \begin{pmatrix} \alpha_{11} & 0 & 0 \\ 0 & \frac{-1}{2}\alpha_{11} & 0 \\ 0 & 0 & \frac{-1}{2}\alpha_{11} \end{pmatrix} = \begin{pmatrix} \frac{2}{3}\alpha & 0 & 0 \\ 0 & \frac{-1}{3}\alpha & 0 \\ 0 & 0 & \frac{-1}{3}\alpha \end{pmatrix}. \tag{12}$$

A new component can be defined: the equivalent backstress $\bar{\alpha}$ for which the components of $\boldsymbol{\alpha}$ are chosen such that $\bar{\alpha} = |\alpha|$. Its expression is the following:

$$\bar{\alpha} = \sqrt{\frac{3}{2}\alpha_{ij}\alpha_{ij}}. \tag{13}$$

For a J_2 Von Mises material, the yield function can thus be written as:

$$f(\boldsymbol{\sigma}, \boldsymbol{\alpha}, \sigma_y^0) = \sqrt{\frac{3}{2}(s_{ij} - \alpha_{ij})(s_{ij} - \alpha_{ij})} - \sigma_y^0 = \bar{\sigma}^{VM} - \sigma_y^0 \leq 0, \tag{14}$$

where $\bar{\sigma}^{VM}$ is the Von Mises effective stress.

Once again, the behavior of the different variables can be studied in the case of a sawtooth loading path.

From 0 to 1.8s, it is the elastic regime as described in the isotropic case. After 1.8s, this is the onset of plasticity: $f(\boldsymbol{\sigma}, \boldsymbol{\alpha}, \sigma_y^0) = 0 \Leftrightarrow \bar{\sigma}^{VM} = \sigma_y^0$ as long as the plasticity occurs. The yield surface is reached and begins to translate as the curve increases in the stress-strain representation (Fig. 10b). Additionally, the equivalent backstress increases due to the evolution of the α_{ij} as described in Eq. 11. An example of such a situation ($t \in [1.8; 2.5]s$) is the orange representation on Fig. 10a. The equivalent plastic strain starts to increase too since there are plastic deformations until it reaches its maximum value $\bar{\varepsilon}^{vp}_{\max} = 0.25\%$ for $\sigma_1 = t_{\max}$ after 2.5s (in yellow on Fig.10a).

Then, the unloading starts and this process is, first, elastically done with $f(\boldsymbol{\sigma}, \boldsymbol{\alpha}, \sigma_y^0) < 0$. The value of σ_{11} decreases and so it is also the case for $\sqrt{\frac{3}{2} s_{ij} s_{ij}}$ and $\bar{\sigma}$. The plastic strain rate is zero and this is the reason why the $\bar{\varepsilon}^p$ and $\bar{\alpha}$ stay constant.

After 6.1s, the material enters once again in plasticity for a compressing load. The yellow ellipse is reached from below this time and starts a downward translation. The equivalent plastic strain restarts increasing because of the plasticity. The value of α, which is the center of the ellipse, decreases and then goes into negative values. On the other hand, the equivalent backstress is always a positive value that decreases until it reaches zero (the center of the ellipse is equal to the center of the *Haigh Westergaard's space*) and starts to climb again.

At t=7.5s, the loading is $-t_{\max}$ and this is represented by the purple curve on Fig. 10a. Then, it is the unloading, the equivalent backstress $\bar{\alpha}$ reaches a new plateau such as the equivalent plastic strain because this unloading is once again elastically done. The point moves on a vertical line inside the ellipse until a new cycle begins.

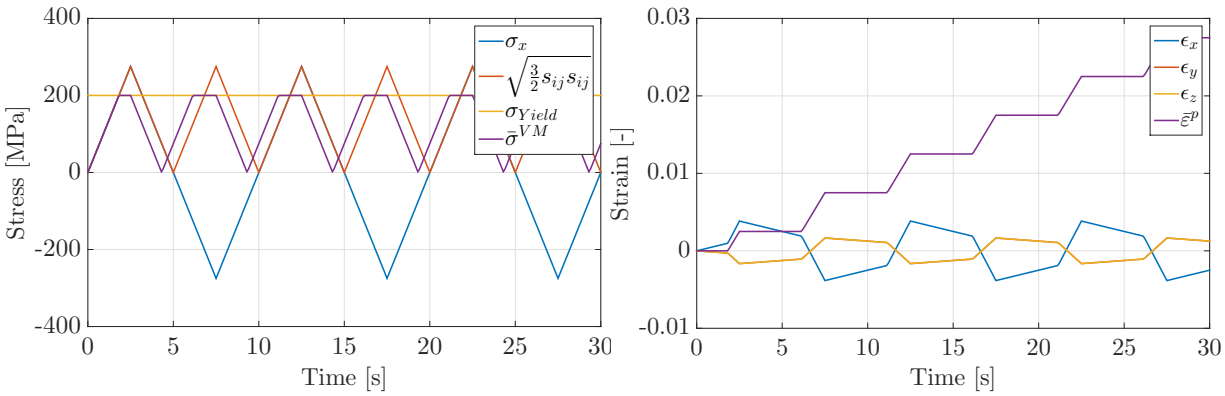

(a) Evolution in time of the stresses.

(b) Evolution in time of the strains.

Figure 8: Linear kinematic hardening model in a plane stress state.

The path followed will always be the one represented by the parallelogram in Fig. 10b and the ellipse will, as a consequence, always move upward and downward between the two extreme cases: the yellow and the purple one. Each time the ellipse is shifted, plasticity occurs, that is the reason why the equivalent plastic strain steps up as a stair without stopping for an infinite number of cycles. Finally, it can be noticed that, when the imposed load is zero at the end of the cycle at 10s, $\sqrt{3J_2} = 0$ but this is not the case for $\bar{\sigma}^{VM}$ because of the non-zero α_{ij} at this stage.

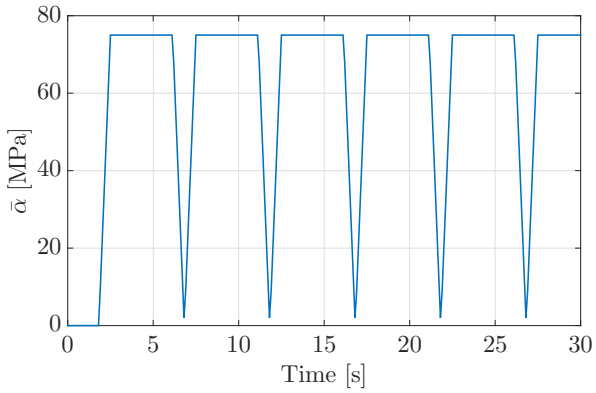

Figure 9: Evolution in time of the equivalent backstress for linear kinematic hardening model in a plane stress state.

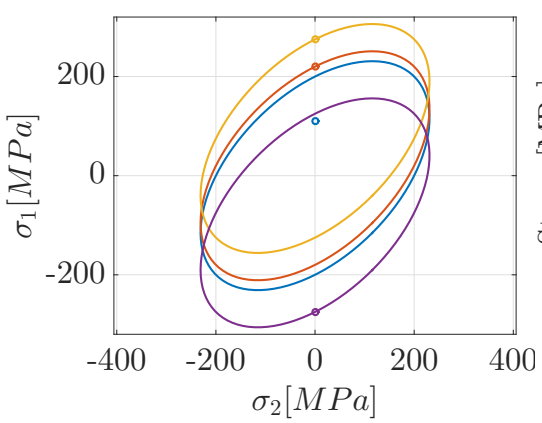

(a) Westergaard's space.

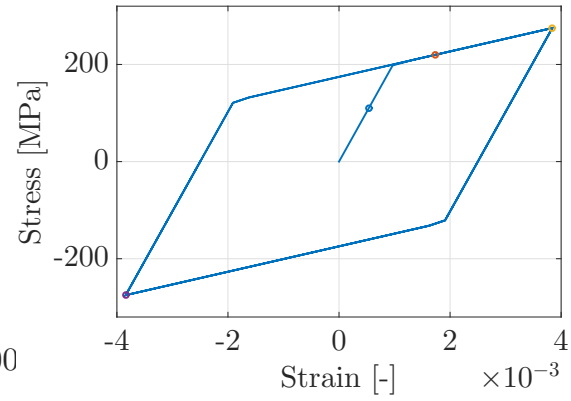

(b) Stress-strain space.

Figure 10: Linear kinematic hardening in a plane stress state
blue dot = 1s, orange dot = 2s, yellow dot = 2.5s, purple dot = 7.5s.

1.4 Linear mixed hardening

In reality, most materials harden both isotropically and kinematically. In this, case the yield surface expands and translates with the plastic deformation as it is simply a mix of the two previous sections. The yield function can thus be written as:

$$f(\boldsymbol{\sigma}, \boldsymbol{\alpha}, \bar{\varepsilon}^p) = \sqrt{\frac{3}{2}(s_{ij} - \alpha_{ij})(s_{ij} - \alpha_{ij})} - \sigma_y(\bar{\varepsilon}^p) = \bar{\sigma}^{VM} - \sigma_y(\bar{\varepsilon}^p) \leq 0. \tag{15}$$

Here again, there exist different laws to describe the evolution of α_{ij} and $\sigma_y(\bar{\varepsilon}^p)$. As only the linear case is analyzed in this section, these two variables are described the same way they were in the previous sections, *i.e.* by Eq. 8 and 11. The hardening coefficient h is subdivided using weights between the isotropic and the kinematic hardening coefficients.

In the case of this study, the values are the following:

$$h_i = \theta^* h = 0.2 \times 30000 = 6000\, MPa \quad \text{and} \quad h_k = (1-\theta^*)h = 0.8 \times 30000 = 24000\, MPa. \tag{16}$$

As it has already been done for the kinematic and isotropic models, the behavior of the important variables can be discussed. Firstly, when the loading starts to increase, the regime is elastic as in the two previous cases. Once again, after 1.8s, the plastic deformation starts. The ellipse is pushed upward and, at the same time, expands uniformly due to the isotropic effects (cf. orange representation in Fig. 12a). This can be explained by both the increase of the subsequent yield stress σ_{yield} and the increase of the equivalent backstress $\bar{\alpha}$. As the deformation is now plastic, the equivalent plastic strain increases also in Fig. 11b. Between 1.8 and 2.5s, $f(\boldsymbol{\sigma}, \boldsymbol{\alpha}, \bar{\varepsilon}^p) = 0 \Leftrightarrow \bar{\sigma}^{VM} = \sigma_y(\bar{\varepsilon}^p)$ even if the two are not represented on the same figure for the sake of clarity.

Once t=2.5s, the loading is equal to $t_{\max}$, $\bar{\varepsilon}^{vp}_{\max}$ is reached and this is represented by the yellow ellipse. Then the unloading starts. The peculiarity of the mixed hardening comes now. Since the ellipse has not only been translated upwards but has also been expanded, the elastic part of the unloading will last longer. Indeed, the material re-enters in plasticity for a lower σ_{11} (i.e. bigger in absolute value). During the elastic unloading, once again, $\bar{\alpha}$ and $\bar{\varepsilon}^p$ are constant.

Since the elastic part lasts longer than before, the plastic part has less time to take place. The onset of plasticity (in compression) starts at 6.4s (against 6.1s for a purely kinematic case), time at which σ_{yield} and $\bar{\varepsilon}^p$ re-start to increase and $\bar{\alpha}$ to decrease. This is done until 7.5s for an applied stress of $-t_{\max}$ which corresponds to the purple ellipse in Fig. 12a. Then the re-loading begins elastically until the end of the cycle.

The specificity of the mixed hardening is here: the plastic deformation will always last less time until the subsequent yield surface reaches an asymptotic value, a kind of limit after an infinite number of cycles. This phenomenon is represented by the reduction of the gaps between the trays in Fig. 11b and 11c. And this is also quite interesting in Fig. 12b. Indeed, the upper and lower parts of the parallelogram are always smaller as the number of cycle increases, this will reach a straight line for an infinite number of loops. At that time, the loading and unloading process from $t_{\max}$ to $-t_{\max}$ will be totally elastic.

Here again, the values of the tensor $\boldsymbol{\alpha}$ are non-zero at the end of a cycle (when $\sigma_{11} = 0$ MPa) and so it is also the case for $\bar{\sigma}^{VM}$. $\sqrt{\frac{3}{2} s_{ij} s_{ij}}$ on the contrary takes a zero value, being equals to $|\sigma_{11}|$ as already mentioned.

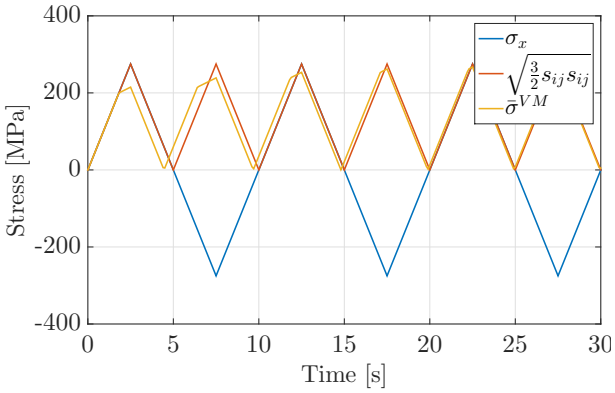

(a) Evolution in time of the stresses.

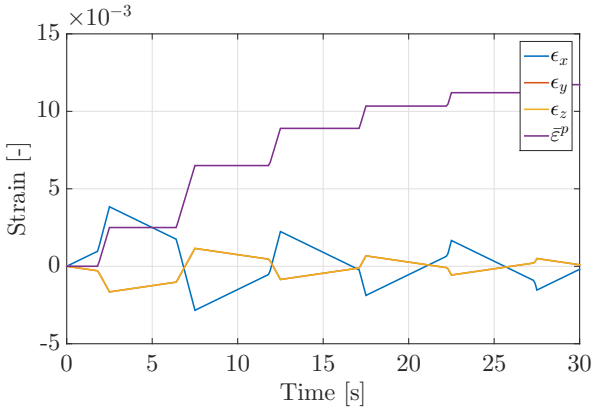

(b) Evolution in time of the strains.

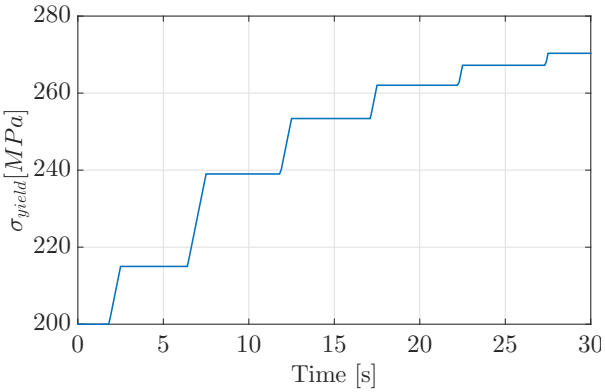

(c) Evolution in time of the yield stress.

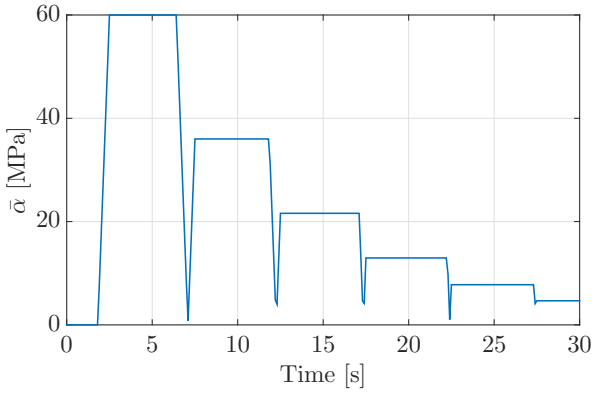

(d) Evolution in time of the equivalent backstress.

Figure 11: Linear mixed hardening in a plane stress state.

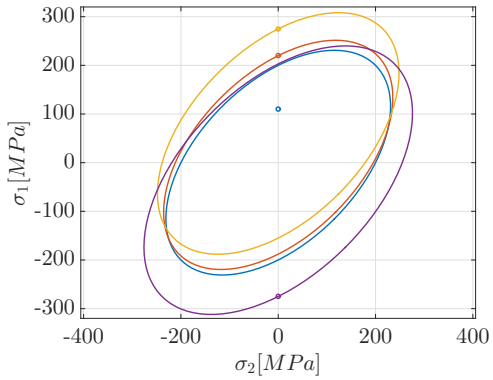

(a) Westergaard's space.

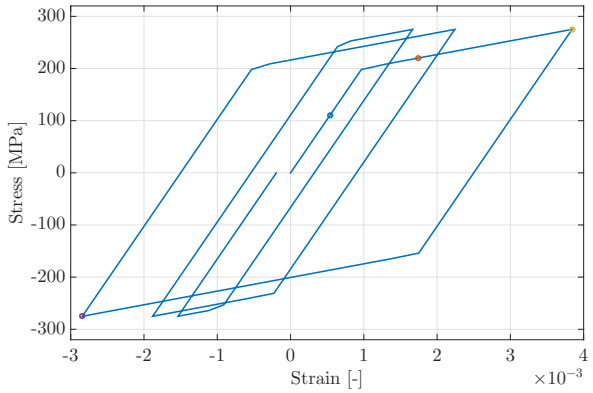

(b) Stress-strain space.

Figure 12: Linear mixed hardening in a plane stress state
blue dot = 1s, orange dot = 2s, yellow dot = 2.5s, purple dot = 7.5s

2 Plane strain state

The same study as presented in the previous section can be performed for a plane strain state. In this configuration, the deformation is allowed along only one direction, in addition to the solicitation direction. An arbitrary choice is to accept the deformation only along $\mathbf{e}_3$. This means that the boundary conditions are slightly modified in comparison with the ones of the plane stress state. Indeed, in addition to the previous boundary conditions, the face number 5 must be blocked along the $\mathbf{e}_2$ direction as shown in Fig. 13 (the blocked faces are the colored ones).

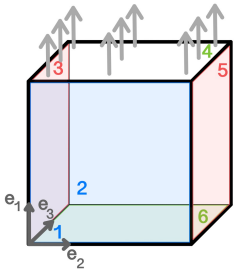

Figure 13: Plane strain state.

This leads to changes in the stress and strain tensors. Indeed, due to the traction or compression along the direction $\boldsymbol{e}_1$, the cube wants to deform in the other two directions (Poisson effect) but it is held back by the imposed conditions. Therefore, this generates an additional stress inside the cube along the blocked direction $\boldsymbol{e}_2$. The stress tensor in the new configuration and the corresponding strain tensor can be respectively deduced:

$$\boldsymbol{\sigma}(t) = \begin{pmatrix} \sigma_{11}(t) & 0 & 0 \\ 0 & \sigma_{22}(t) & 0 \\ 0 & 0 & 0 \end{pmatrix} \quad \text{and} \quad \boldsymbol{\varepsilon}(t) = \begin{pmatrix} \varepsilon_{11}(t) & 0 & 0 \\ 0 & 0 & 0 \\ 0 & 0 & \varepsilon_{33}(t) \end{pmatrix}.$$

For the cube in plane strain state, the stress deviatoric $\boldsymbol{s}$ tensor can also be computed:

$$\boldsymbol{s} = \text{dev}(\boldsymbol{\sigma}) = \boldsymbol{\sigma} - \frac{1}{3}\text{tr}(\boldsymbol{\sigma}) \tag{17}$$

$$\Leftrightarrow \boldsymbol{s}(t) = \begin{pmatrix} \frac{2}{3}\sigma_{11}(t) - \frac{1}{3}\sigma_{22}(t) & 0 & 0 \\ 0 & -\frac{1}{3}\sigma_{11}(t) + \frac{2}{3}\sigma_{22}(t) & 0 \\ 0 & 0 & -\frac{1}{3}\sigma_{11}(t) - \frac{1}{3}\sigma_{22}(t) \end{pmatrix}. \tag{18}$$

In elasticity, σ_{22} can be expressed as a function of σ_{11} thanks to the Hooke's law:

$$\begin{pmatrix} \sigma_{11} \\ \sigma_{22} \\ 0 \end{pmatrix} = \frac{E}{(1+\nu)(1-2\nu)} \begin{pmatrix} 1-\nu & \nu & 0 \\ \nu & 1-\nu & 0 \\ 0 & 0 & 1-2\nu \end{pmatrix} \begin{pmatrix} \varepsilon_{11} \\ 0 \\ \varepsilon_{33} \end{pmatrix}. \tag{19}$$

Thanks to this, the following system is obtained:

$$\sigma_{22} = \frac{\nu E}{(1-2\nu)(1+\nu)}(\varepsilon_{11}+\varepsilon_{33}), \quad \varepsilon_{11} = \frac{(1+\nu)}{E}(1-\nu)\sigma_{11}, \quad \varepsilon_{33} = \frac{(1+\nu)}{E}(-\nu\sigma_{11}) \tag{20}$$

$$\Leftrightarrow \sigma_{22} = \nu\sigma_{11}. \tag{21}$$

In case of plasticity, even if σ_{11} passes from t_{max} to $-t_{max}$, $\sqrt{3J_2} = \sqrt{\frac{3}{2}s_{ij}s_{ij}}$ will not

pass through a zero value (cf. Fig. 14a). In fact, this value can be computed as:

$$\sqrt{3J_2} = \sqrt{\frac{3}{2}s_{ij}s_{ij}} = \sqrt{\frac{3}{2}((\frac{2}{3}\sigma_{11} - \frac{1}{3}\sigma_{22})^2 + (-\frac{1}{3}\sigma_{11} + \frac{2}{3}\sigma_{22})^2 + (-\frac{1}{3}\sigma_{11} - \frac{1}{3}\sigma_{22})^2)} \quad (22)$$

$$= \sqrt{\sigma_{11}^2 - \sigma_{11}\sigma_{22} + \sigma_{22}^2}. \quad (23)$$

Indeed, when there is hardening, the plane strain state is much more complicated than the plane stress state. Residual stresses will appear and this value will not vanish and always stay positive: even if $\sigma_{11} = 0$ MPa, σ_{22} will not take a zero value at the same time except in the perfectly plastic case. This complexity is the reason why only the effective values will be studied here bellow. Additionally, since the stress tensor is more complex now, the representation of the yield surface in the *Haigh Westergaard's space* will be done using the deviatoric plane where the yield surface is represented by a circle of radius $\sqrt{\frac{2}{3}}\sigma_{yield}$. To avoid redundancy, this study will be more concise than the previous one.

2.1 Perfectly plastic model

As it has been said previously, a material is perfectly plastic when there is no hardening at all. The yield criterion can be written, in the case of a Von-Mises J_2 material, as described in Eq. 7. By putting Eq. 23 in the yield criterion, one gets:

$$f = \sqrt{\sigma_{11}^2 - \sigma_{11}\sigma_{22} + \sigma_{22}^2} - \sigma_y^0 = 0 \Leftrightarrow \sqrt{\sigma_{11}^2 - \sigma_{11}\sigma_{22} + \sigma_{22}^2} = \sigma_y^0. \quad (24)$$

By using Metafor, the same problem as in the perfectly plastic model in the plane stress state is encountered: the software is not able to represent this kind of stress driven problem.

2.2 Linear isotropic hardening

If the isotropic model presented in Section 1.2 is applied on the cube in plane strain state, the Eq. 8 and 9 being still verified, the evolution of the different variables can be investigated. It is important to notice that the expression of the stress deviatoric tensor $\boldsymbol{s}$ is now different and thus the behavior of $\bar{\sigma} = \sqrt{\frac{3}{2}s_{ij}s_{ij}}$ is different too.

One can see that the behavior of the other parameters is very similar to what has been obtained in Section 1.2. Indeed, the yield stress σ_{yield} and the plastic strain $\bar{\varepsilon}^p$ are constant the first 2 seconds. It is the elastic domain (in blue in Fig. 15). Then, it is the onset of plasticity, and both variables start to increase with $f = 0 \Leftrightarrow \sigma_{yield} = \bar{\sigma}$ until $\sigma_{11} = t_{\max}$ (in yellow in Fig. 15). The particularity of the plane strain is that, at the end of the compression loading, due to complex phenomena linked to additional stresses, plasticity will once again occur in the first cycle. This is the reason why there is one more step in the representation of σ_{yield} and of $\bar{\varepsilon}^p$ (in purple in Fig. 15). But then, the loading and unloading will always be elastic processes. As in the plane stress state.

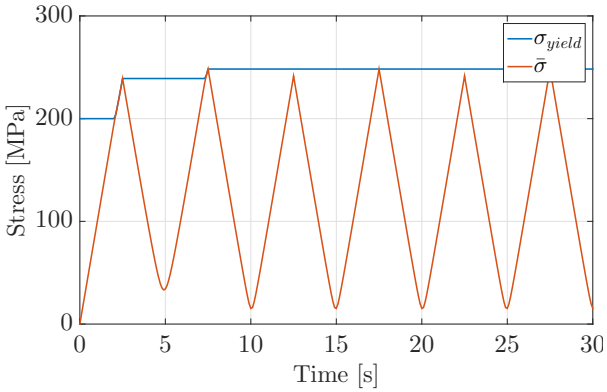

(a) Evolution in time of the stresses.

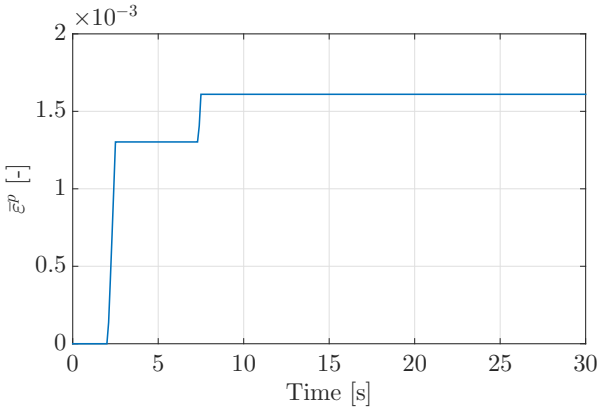

(b) Evolution in time of the equivalent plastic strain.

Figure 14: Linear isotropic hardening in a plane strain state.

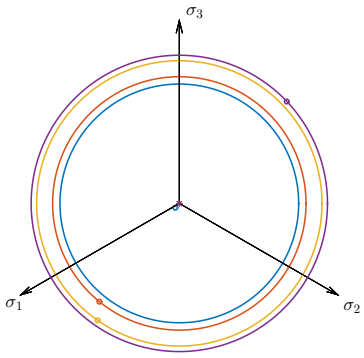

Figure 15: Westergaard's space.

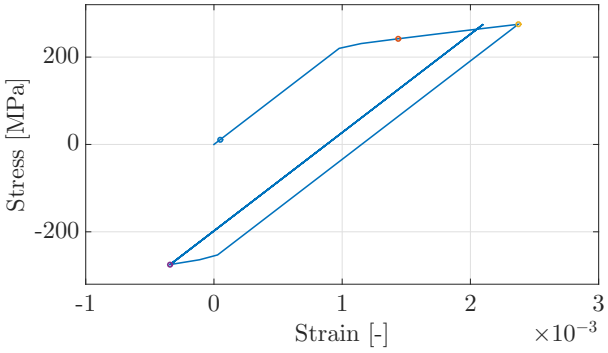

Figure 16: Stress-strain space.

Figure 17: Linear isotropic hardening in a plane strain state
blue dot = 1s, orange dot = 2.2s, yellow dot = 2.5s, purple dot = 7.5s.

2.3 Linear kinematic hardening

The linear kinematic hardening model described in Section 1.3 is applied on the cube in plane strain state. Once again, only the differences with the plane stress state will be raised. However, one can notice that the evolution of the parameters is very similar to the plane stress case here. In fact, during the two first seconds, this is the elastic domain: $f < 0$, $\bar{\varepsilon}^p = 0$ and $\bar{\alpha} = 0$ (represented in blue in Fig. 19a). Then plasticity begins, $\bar{\varepsilon}^p$ and $\bar{\alpha}$ increase with $f = 0$ (thus with $\bar{\sigma}^{VM} = \sigma_{yield}$ constant) until $\sigma_{11} = t_{\max}$ at 2.5 seconds. During this plasticity, the center of the yield surface in the *Haigh Westergaard's space* moves vertically. The phenomenon has nothing different than in the plane stress state: when the unloading starts, it is first elastically done and then, the plasticity occurs and the ellipse starts to move downward until $\sigma_{11} = -t_{\max}$ with a re-increasing in Fig. 18b and in $\bar{\alpha}$ which has the same shape as in Fig. 9. From $-t_{\max}$ to 0 MPa, the loading is elastic. Then, for the next cycles, the yield surface will always be shifted when plasticity

occurs in traction and in compression. There is no important differences compared to the plane stress case except the expression of the stress deviatoric tensor $\boldsymbol{s}$ and thus the evolution of $\sqrt{\frac{3}{2}s_{ij}s_{ij}}$ and $\bar{\sigma}^{VM}$. Once again, due to the non-zero $\boldsymbol{\alpha}$ when $\sigma_{11} = 0\,MPa$, $\bar{\sigma}^{VM}$ does not vanish either.

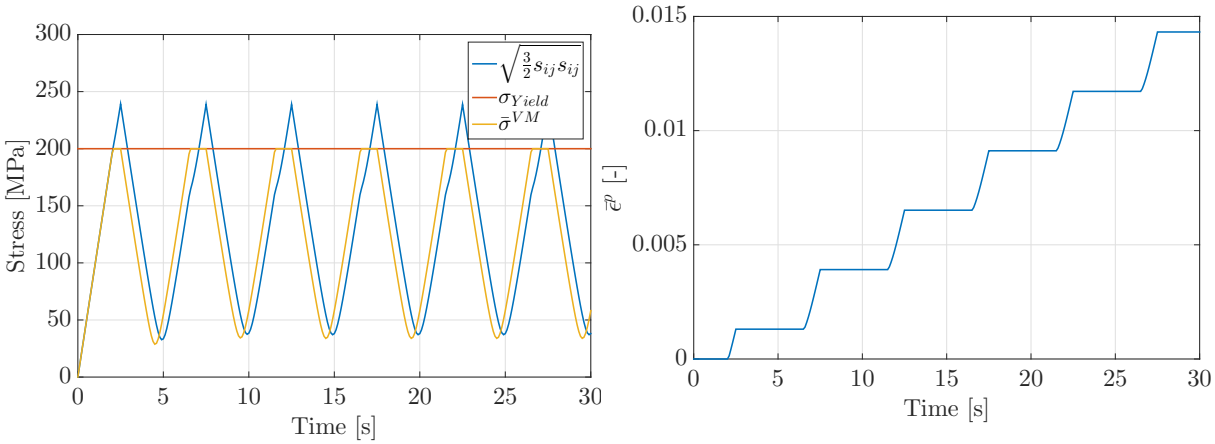

(a) Evolution in time of the stresses.

(b) Evolution in time of the equivalent plastic strain.

Figure 18: Linear kinematic hardening in a plane strain state.

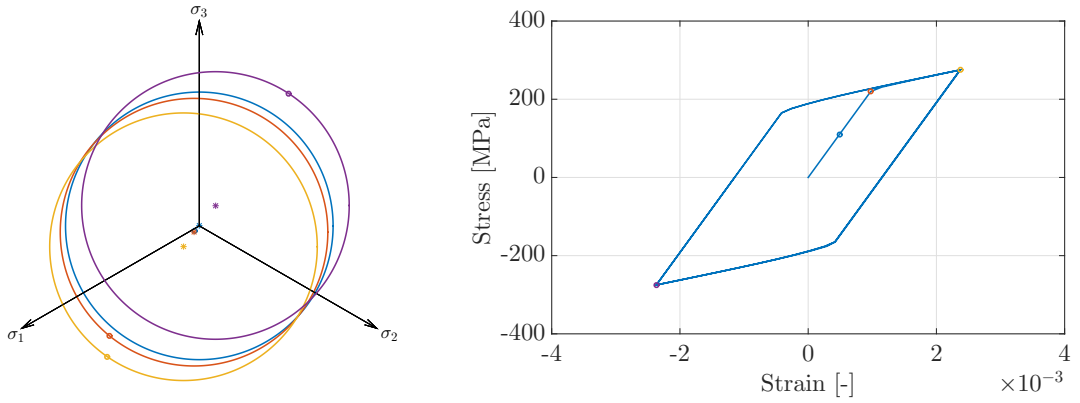

(a) Westergaard's space.

(b) Stress-strain space.

Figure 19: Linear kinematic hardening in a plane strain state
blue dot = 1s, orange dot = 2.2s, yellow dot = 2.5s, purple dot = 7.5s.

2.4 Linear mixed hardening

Finally, the linear mixed hardening model can be applied on the cube in a plane strain state. This more realistic model is described in details by Eq. 15 and 16.

First, the elastic regime takes place as in the previous models. When the yield criterion is met after 2 seconds, the yield surface in the *Haigh Westergaard's space* starts to move upward and to expand due to the kinematic and isotropic effects respectively. During plasticity, $f = 0$ thus $\bar{\sigma}^{VM} = \sigma_{yield}$ but this last one is no longer constant due to the

isotropic hardening. That is the reason why $\bar{\sigma}^{VM}$ is not constant during the plastic deformation in Fig. 20a. After 2.5 seconds, the unloading starts. As in the plane stress case, the plasticity will take longer to be activated due to the expansion. That is the reason why, at each cycle as already described for the plane stress case, the plasticity will always last for a shorter period. And once again, the yield surface will tend to an asymptotic value for an infinite number of cycles.

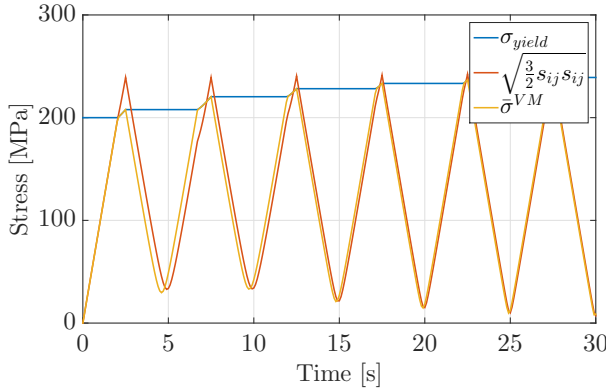

(a) Evolution in time of the stresses.

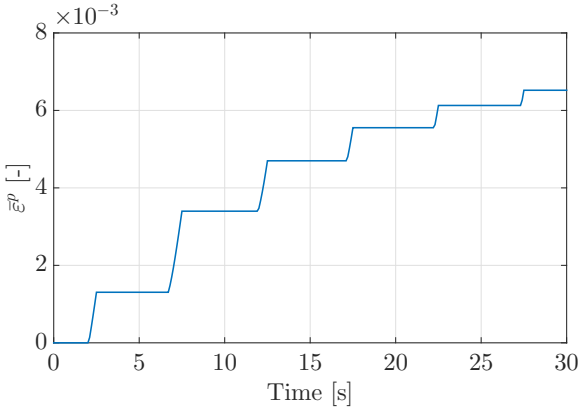

(b) Evolution in time of $\bar{\varepsilon}^p$.

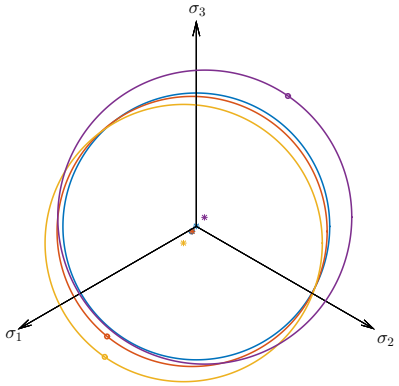

(c) Westergaard's space.

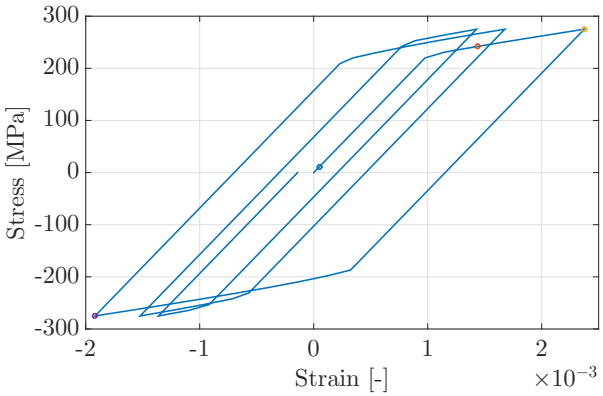

(d) Stress-strain space.

Figure 20: Linear mixed hardening in a plane strain state
blue dot = 1s, orange dot = 2.2s, yellow dot = 2.5s, purple dot = 7.5s.

3 Global discussion

In this section, some additional discussions will be lead for both plane stress and plane strain states.

3.1 Plastic strain

One can notice that whatever the linear hardening model, the equivalent plastic strain $\bar{\varepsilon}^p$ reaches always $\bar{\varepsilon}^p_{\max}$ when the load reaches $\sigma_{11} = t_{\max}$ for the first time in the case of a plane stress state for the cube. However, this is not the case for the plane strain case. This particularity will be explained hereafter.

Firstly, the effective plastic strain rate can be written thanks to the strain rate tensor $\boldsymbol{D}$:

$$\dot{\bar{\varepsilon}}^p = \sqrt{\frac{2}{3} D^p_{ij} D^p_{ij}} = \sqrt{\frac{2}{3} \lambda N_{ij} \lambda N_{ij}} = \sqrt{\frac{2}{3}} \lambda, \tag{25}$$

where $\boldsymbol{N}$ is the unit tensor which is the normal to the yield surface and λ the intensity of the plastic flow, also called the plastic multiplier. This parameter can be re-expressed by one of the Prandtl-Reuss equations for a J_2 Von-Mises material obtained thanks to the consistency equation:

$$\lambda = \frac{\frac{\partial f}{\partial s_{ij}} \mathbb{H}_{ijkl} D_{kl}}{\frac{\partial f}{\partial s_{pq}} \mathbb{H}_{pqtu} N_{tu} - \frac{\partial f}{\partial \boldsymbol{q}^{(v)}} * r^{(v)}(\boldsymbol{\sigma}, \boldsymbol{q})} \overset{J_2 \text{ V-M with associated flow rule}}{\Rightarrow} \lambda = \frac{N_{kl} D_{kl}}{1 + \frac{h}{3G}}, \tag{26}$$

where the hardening coefficient is $h = h_i + h_k$ and the shear modulus $G = \frac{E}{2(1+\nu)}$.

For a given state (plane stress or plane strain), D_{kl} will take the same value whatever the hardening model. Indeed, the evolution of the stress components can be expressed as $\dot{\sigma}_{ij} = \mathbb{M}_{ijkl} D_{kl}$ where the tensor $\mathbb{M}$ characterizes the material behavior, taking into account the stress history. However, for the first loading, the stress history of the material is the same for every model since the subsequent yield stress that limits the entry in plasticity is equal to the virgin yield stress σ^0_y. As a consequence, the strain rate tensor D_{kl} will be the same for the first entry in plasticity.

In the case of a plane stress state, the unit normal to the yield surface N_{ij} is a constant because there is only a loading/unloading in the $\boldsymbol{e}_1$ direction. So that the N_{ij} components will be the same for all the different hardening models even if the yield surface is translated and/or expanded. On the other hand, for a plane strain case, the stresses evolve in two directions $\boldsymbol{e}_1$ and $\boldsymbol{e}_2$ so that, when plasticity occurs even for the first time, the yield surface is expanded and/or translated in two directions at the same time so that the unit normal varies in different ways as a function of the hardening model used.

3.2 Plastic dissipation

The plastic dissipation rate is expressed as:

$$\mathbb{D} = \sigma_{ij} D^p_{ij} = \sigma : \boldsymbol{D}^p = \bar{\sigma} \dot{\bar{\varepsilon}}^p \tag{27}$$

and gives the rate at which the energy is dissipated due to the movement of the atomic planes at the microscopic level. This is also the time derivative of the inelastic work:

$$\mathbb{D} = \dot{W}^{in} \quad \text{with} \quad W^{in} = \int \sigma_{ij} D^p_{ij} \mathrm{d}t. \tag{28}$$

Indeed, the inelastic work is defined as the energy dissipated by the plastic deformation.

These values are displayed as a function of time for the plane stress state in Fig. 21a and 21b. In this particular case, the dissipation rate can be re-expressed thanks to Eq. 27 as:

$$\mathbb{D} = \sigma_{11} D^p_{11} = \bar{\sigma} \dot{\bar{\varepsilon}}^p. \tag{29}$$

One can see that the plastic strain rate $\mathbb{D}$ is zero when $\bar{\varepsilon}^p$ is constant because in this case, the regime is elastic and thus D^p_{11} is zero too. When plasticity occurs, the effective strain increases linearly (cf. Section 1 and 2) and thus the plastic dissipation rate is a positive value. This value is only a constant plateau in the kinematic hardening model for which the effective stress $\bar{\sigma}^{VM}$ does not vary as a function of $\bar{\varepsilon}^p$ during plasticity. On the other hand, one can notice that, in the case of kinematic hardening, the plastic dissipation tends to become always bigger when the number of cycles increases until reaching the infinity unlike other models that tend towards a finite constant value.

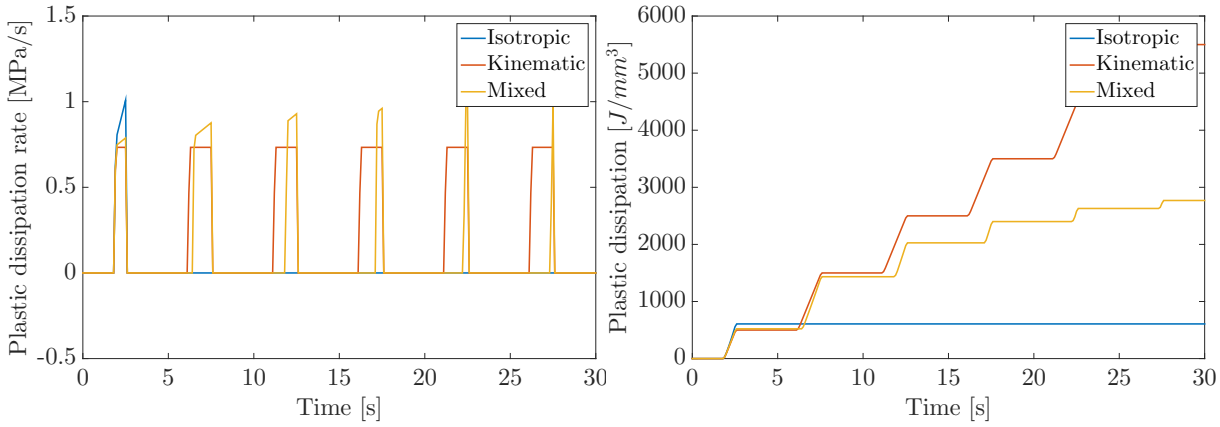

(a) $\mathbb{D}$ as a function of time.

(b) W^{in} as a function of time.

Figure 21: Plane stress state.

In addition to this, these values are also displayed as a function of time for the plane strain state in Fig. 22a and 22b. In this case, the dissipation rate can be re-expressed thanks to Eq. 27 as:

$$\mathbb{D} = \sigma_{11} D^p_{11} + \sigma_{22} D^p_{22} = \bar{\sigma}\dot{\bar{\varepsilon}}^p. \tag{30}$$

This expression is more complex than in the plane stress state, that is the reason why the plastic dissipation rate with kinematic hardening does not reach a constant plateau when there is plasticity. The only difference with the previous case is the second tray obtained for the isotropic model in Fig. 21b. This is due to the second plasticity entry as explained before.

Finally, while looking more carefully on these graphs, one can see that the plastic dissipation is more important in the plane stress state. This is due to the Poisson effect that dissipates some energy and that does not take place in the plane strain case due to the boundary conditions.

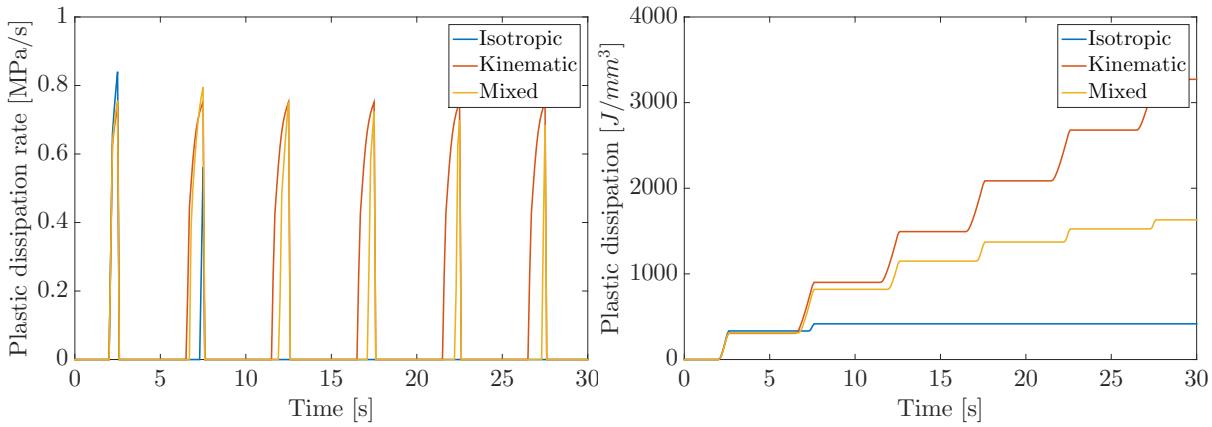

(a) $\mathbb{D}$ as a function of time.

(b) W^{in} as a function of time.

Figure 22: Plane strain state.

3.3 Load reversal

If the load direction is inverted, it means if the applied load is now $\sigma_{11}(t) = -\sigma_{11}(t)$, the results are similar to those obtained in the previous Sections 1 and 2. The only noticeable difference is that the variables (except the non-signed variables as $\bar{\sigma}$, σ_{Yield}, $\sqrt{\frac{3}{2}s_{ij}s_{ij}}$ and $\bar{\varepsilon^p}$) are of opposite sign, the graphs are symmetric with the abscissa axis. The results in the *Haigh Westergaard's space* and in the stress-strain space are similar but the loading path are inverted.

Part II
Elasto-plastic behavior with non-linear hardening

In this second section, non-linear hardening laws will be considered. First non-linear kinematic hardening will be studied thanks to the *Armstrong Frederick's* model and the influence of the dynamic recovery parameter η_k will be analyzed. Then, different mixed hardening laws will be compared. All numerical results will be discussed in parallel with the theoretical concepts.

4 Influence of the dynamic recovery parameter

In order to better fit with experimental results of cyclic loading tests, the linear kinematic hardening model of *Melan and Prager* presented in previous sections can be improved by adding a dynamic term. Therefore, *Armstrong and Frederick* introduced the dynamic recovery parameter η_k to represent the dynamic fading memory of the material and to better reproduce the *Bauschinger effect*. The evolution of the backstress is thus given by the law:

$$\dot{\alpha}_{ij} = \frac{2}{3} h_k D^p_{ij} - \eta_k \dot{\bar{\varepsilon}}^p \alpha_{ij}. \tag{31}$$

For purely kinematic hardening, the yield stress σ^0_y does not evolve so that the yield surface is only modified by the moving position of its center $\boldsymbol{\alpha}$.

The parameter η_k is dimensionless. Indeed the effective plastic strain $\bar{\varepsilon}^p$ has no dimension so that $\dot{\bar{\varepsilon}}^p \alpha_{ij}$ are in MPa/s, as well as $\dot{\alpha}_{ij}$.

From Eq. 31, it can be seen that the evolution of the backstress results from the competition between two forces. The first term of Eq. 31 is the force that tends to move the center of the yield surface in the direction of the plastic strain rate, it is the driving effect. The second term may be interpreted as a recovery force that has the tendency to bring back $\boldsymbol{\alpha}$ to its original position.

Two theoretical limit cases of the parameter η_k can already be highlighted:

- $\eta_k = 0$: The dynamic recovery has no influence and the behavior of the material will be the one described by the linear kinematic hardening exposed previously.
- $\eta_k \gg$: The restoring force become so important that the backstress can not evolve. As neither the yield stress nor the backstress is modified, the model degenerates to the perfectly plastic case described in Section 1.1.

4.1 Evolution laws of the hardening parameter q

The internal variables contained in $\mathbf{q}$ reflect the memory of the material. When plastic deformation occurs, $\mathbf{q}$ evolves and the history of the deformations can thus be taken into

account. The evolution laws of these internal parameters take the following general form:

$$\dot{\mathbf{q}}^{(k)} = \lambda\, r^{(k)}(\boldsymbol{\sigma}, \mathbf{q}), \tag{32}$$

where λ is the flow intensity (or plastic multiplier) and $r^{(k)}$ depends on the hardening model used to describe plasticity.

The three evolution rules mentioned in this report are the following:

- Isotropic hardening : $r(\boldsymbol{\sigma}, \bar{\varepsilon}^p) = \sqrt{\frac{2}{3}}$.
- Linear kinematic hardening (M-P model) : $r(\boldsymbol{\sigma}, \alpha_{ij}) = \frac{2}{3}\, h_k\, N_{ij}$.
- Non-linear kinematic hardening (A-F model) : $r(\boldsymbol{\sigma}, \alpha_{ij}) = \frac{2}{3}\, h_k\, N_{ij} - \sqrt{\frac{2}{3}}\, \eta_k\, \alpha_{ij}$.

It can be noted that for isotropic hardening, the function r is the same for both linear and non-linea rmodels as $\dot{\bar{\varepsilon}}^p = \sqrt{\frac{2}{3}}\,\lambda$. However, the evolution $\sigma_y(\bar{\varepsilon}^p)$ will depend on the hardening law.

4.2 Asymptotic value of the backstress

When the plastic deformation becomes very large, the linear term of Eq. 31 tends to move the center of the yield surface very far from the origin. At the same time, the recovery force increases with the backstress to bring back the center of the yield surface to its initial position. There is thus a competition between the two forces. The backstress reaches its asymptotic value α_{ij}^u when $\dot{\alpha}_{ij} = 0$, *i.e* when the two forces balance each other. From Eq. 31, it comes:

$$\dot{\alpha}_{ij} = 0 \quad \Rightarrow \qquad \alpha_{ij}^u = \frac{\frac{2}{3}\, h_k\, D_{ij}^p}{\eta_k\, \dot{\bar{\varepsilon}}^p}. \tag{33}$$

Using the fact that $D_{ij}^p = \lambda\, N_{ij}$ and the definition of $\dot{\bar{\varepsilon}}^p$ (Eq. 25), it comes:

$$\alpha_{ij}^u = \sqrt{\frac{3}{2}}\, \frac{h_k}{\eta_k}\, N_{ij}, \tag{34}$$

$$\bar{\alpha}^u = \sqrt{\frac{2}{3} \alpha_{ij}^u\, \alpha_{ij}^u} = \frac{h_k}{\eta_k}. \tag{35}$$

In case of purely kinematic hardening, the yield criterion is

$$f = \sqrt{\frac{3}{2}(s_{ij} - \alpha_{ij})(s_{ij} - \alpha_{ij})} - \sigma_y^0 \leq 0 \tag{36}$$

and taking the form of the deviatoric stress tensor $\boldsymbol{s}$ and of the backstress tensor $\boldsymbol{\alpha}$ under the plane stress assumption into account (respectively Eq. 5 and Eq. 12), one can get:

$$f = |\sigma - \alpha| - \sigma_y^0 \leq 0. \tag{37}$$

The limit value for η_k can be determined by evaluating the condition of Eq. 37 at the maximum traction point (the maximum compression point would give the same results),

i.e. when $\sigma = \sigma_{11} = t_{\max} = 275$ MPa.

$$\begin{aligned} t_{\max} - \sigma_y^0 \;&\leq\; \alpha^u = \frac{h_k}{\eta_k}, \\ \eta_{k,\max} \;&\leq \frac{h_k}{t_{\max} - \sigma_y^0} = \frac{30\,000 \text{ MPa}}{75 \text{ MPa}} = 400. \end{aligned} \tag{38}$$

As a conclusion, if η_k increases, the recovery force becomes larger and the maximum value that the backstress can take decreases. The hardening phenomenon is less important and the amplitude of the force that the material can bear decreases.

4.3 Generalized plastic modulus H^p for non-linear mixed hardening

During plastic deformation, the consistency condition (cf. Eq. 39) must be satisfied. This condition express the fact that the yield criterion is fulfilled during all the plastic process.

$$\dot{f} = \frac{\partial f}{\partial \sigma_{ij}}\, \dot{\sigma}_{ij} + \frac{\partial f}{\partial \mathbf{q}^{(k)}} * \dot{\mathbf{q}}^{(k)} = 0. \tag{39}$$

Using the internal parameters variation laws under the form of Eq. 32, the consistency condition can be rewritten as:

$$\dot{f} = \frac{\partial f}{\partial \sigma_{ij}}\, \dot{\sigma}_{ij} - H^p\, \lambda,$$

where the generalized plastic modulus H^p is defined as:

$$H^p = -\frac{\partial f}{\partial \boldsymbol{q}^{(k)}} * r^{(k)}(\boldsymbol{\sigma}, \boldsymbol{q}). \tag{40}$$

In the case of a mixed non-linearhardening, the yield criterion is written as:

$$f = \sqrt{\frac{3}{2}(s_{ij} - \alpha_{ij})(s_{ij} - \alpha_{ij})} - \sigma_y(\bar{\varepsilon}^p) \leq 0, \tag{41}$$

where the evolution of α_{ij} is given by the *Amstrong-Frederick's* model (Eq. 31) and the evolution of the yield stress is given by the *Voce's* saturated law:

$$\sigma_y = \sigma_y^0 + (\sigma_y^\infty - \sigma_y^0)\, \left(1 - \exp\left\{\frac{-h_i\, \bar{\varepsilon}^p}{\sigma_y^\infty - \sigma_y^0}\right\}\right). \tag{42}$$

Therefore, two internal parameters are needed in this model to take the loading history into account: α_{ij} and $\bar{\varepsilon}^p$, their evolution rules are mentioned in Section 4.1. The

generalized plastic modulus becomes:

$$H^p = -\frac{\partial f}{\partial \alpha_{ij}} r(\boldsymbol{\sigma}, \alpha_{ij}) - \frac{\partial f}{\partial \bar{\varepsilon}^p} r(\boldsymbol{\sigma}, \bar{\varepsilon}^p), \tag{43}$$

$$H^p = \frac{\sqrt{\frac{3}{2}}(s_{ij} - \alpha_{ij})}{\sqrt{(s_{ij} - \alpha_{ij})(s_{ij} - \alpha_{ij})}} \left(\frac{2}{3} h_k N_{ij} - \sqrt{\frac{2}{3}} \eta_k \alpha_{ij} \right) + \sqrt{\frac{2}{3}} h_i \exp \left\{ \frac{-h_i \, \bar{\varepsilon}^p}{\sigma_y^\infty - \sigma_y^0} \right\}. \tag{44}$$

In Eq. 44, appears the plastic flow direction N_{ij} defined as:

$$N_{ij} = \frac{\frac{\partial g}{\partial \sigma_{ij}}}{\sqrt{\frac{\partial g}{\partial \boldsymbol{\sigma}} : \frac{\partial g}{\partial \boldsymbol{\sigma}}}}, \tag{45}$$

where g is the plastic flow potential. Focusing on stable materials in *Drucker's* sense, the assumption of associated flow can be made, *i.e.* $g(\boldsymbol{\sigma}, \boldsymbol{q}) = f(\boldsymbol{\sigma}, \boldsymbol{q})$. Moreover, since the pressure has no influence on plasticity, the derivative of f with respect to σ_{ij} can be replaced by the derivative of f with respect to the deviatoric components of the stress s_{ij}.

$$\frac{\partial f}{\partial s_{ij}} \overset{\text{Eq. 41}}{=} \frac{3}{2} \frac{s_{ij} - \alpha_{ij}}{\sqrt{\frac{3}{2}(s_{ij} - \alpha_{ij})(s_{ij} - \alpha_{ij})}} \quad \overset{\text{Eq. 45}}{\Longleftrightarrow} \quad N_{ij} = \frac{\phi_{ij}}{\sqrt{\boldsymbol{\phi} : \boldsymbol{\phi}}} = \frac{s_{ij} - \alpha_{ij}}{\sqrt{(\boldsymbol{s} - \boldsymbol{\alpha}) : (\boldsymbol{s} - \boldsymbol{\alpha})}}. \tag{46}$$

Inserting Eq. 46 in Eq. 44 and using the total hardening parameter h (cf. Eq. 16), the demonstration can finally be ended:

$$H^p = \sqrt{\frac{2}{3}}(1 - \theta) \, h - \eta_k \underbrace{\frac{s_{ij} - \alpha_{ij}}{\sqrt{(\boldsymbol{s} - \boldsymbol{\alpha}) : (\boldsymbol{s} - \boldsymbol{\alpha})}}}_{= N_{ij}} \alpha_{ij} + \sqrt{\frac{2}{3}} \, \theta \, h \, \exp \frac{-\theta \, h \, \bar{\varepsilon}^p}{\sigma_y^\infty - \sigma_y^0} \tag{47}$$

$$= \sqrt{\frac{2}{3}} \, (1 - \theta) \, h - \eta_k \, \frac{(\boldsymbol{s} - \boldsymbol{\alpha}) : \boldsymbol{\alpha}}{\sqrt{(\boldsymbol{s} - \boldsymbol{\alpha}) : (\boldsymbol{s} - \boldsymbol{\alpha})}} + \sqrt{\frac{2}{3}} \, \theta \, h \, \exp \frac{-\theta \, h \, \bar{\varepsilon}^p}{\sigma_y^\infty - \sigma_y^0}. \tag{48}$$

From Eq. 47 and 48, it can be seen that the influence of the recovery term can be analyzed by studying the evolution of the term $(\boldsymbol{s} - \boldsymbol{\alpha}) : \boldsymbol{\alpha}$ in *Haigh Westergaard's space*. Because this term has only an influence on the non-linear kinematic hardening, the following discussion will focus on this law ($\theta = 0$). Further analysis with mixed hardening will be performed in the next sections. The generalized plastic modulus in the case of a purely non-linear kinematic hardening becomes thus:

$$H^p = \sqrt{\frac{2}{3}} h_k - \eta_k \frac{(\boldsymbol{s} - \boldsymbol{\alpha}) : \boldsymbol{\alpha}}{\sqrt{(\boldsymbol{s} - \boldsymbol{\alpha}) : (\boldsymbol{s} - \boldsymbol{\alpha})}}. \tag{49}$$

For the plane stress problem studied here (loading in the σ_1-direction), the deviatoric stress tensor $\boldsymbol{s}$ and the backstress tensor $\boldsymbol{\alpha}$ have the form of Eq. 5 and Eq. 12, thus H^p

is finally:

$$H^p = \sqrt{\frac{2}{3}} h_k - \sqrt{\frac{2}{3}} \eta_k \, \alpha \, \frac{(\sigma - \alpha)}{|\sigma - \alpha|}. \tag{50}$$

This expression can easily be interpreted in *Haigh Westergaard's space*. Indeed the diagonal of $\boldsymbol{s}$ and $\boldsymbol{\alpha}$ have respectively the components $\left(\frac{2\sigma}{3} \; \frac{-\sigma}{3} \; \frac{-\sigma}{3}\right)$ and $\left(\frac{2\alpha}{3} \; \frac{-\alpha}{3} \; \frac{-\alpha}{3}\right)$ in the 3D space of principal stresses. They are therefore projected in the σ_1-direction of the deviatoric plane with the components $(\sigma \, 0 \, 0)$ and $(\alpha \, 0 \, 0)$.

The influence of the non-linear kinematic hardening term can be analyzed at the crucial points of the loading cycle presented in Fig. 23. It will result in four different cases : the traction loading (Fig. 24) and the compression loading (Fig. 25), each divided as a function of the position of the backstress.

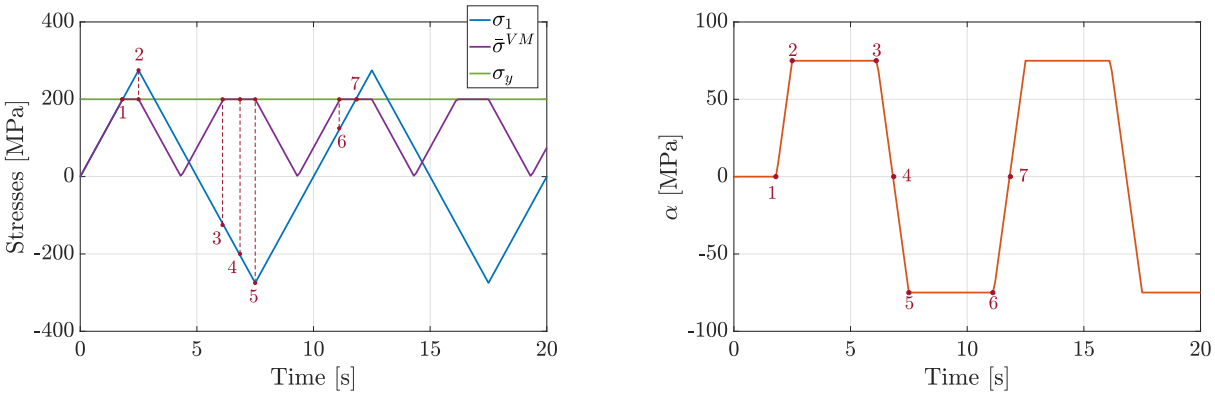

(a) Evolution of the stresses.

(b) Evolution of the backstress α.

Figure 23: Evolution in time of the stresses and backstress during a loading cycle and identification of the crucial points.

During the first traction plastic loading (from point 1 to 2 in Fig. 23), the center of the yield surface is shifted ahead the plane $O\sigma_2\sigma_3$. This corresponds to the case of Fig. 24a, in which one can see that α and $\sigma - \alpha$ are both positive. While the traction increases, the center of the yield surface will move further in the σ_1-direction and α will increase. As a consequence, the generalized plastic modulus H^p decreases from its initial value when plasticity starts ($\alpha = 0$) $H_1^p = \sqrt{2/3}\, h_k$ to its minimum value when the traction loading reaches its maximum (point 2) :

$$H_2^p = H_{\min}^p = \sqrt{\frac{2}{3}} \, (h_k - \eta_k \, \alpha_{\max}). \tag{51}$$

The dynamic recovery term has thus the effect of slowing down the motion of the yield surface center, the further this one from the origin, the greater this effect.

Then, between points 2 and 3, the elastic unloading and the elastic compression loading occur. During those elastic processes, the yield surface does not move, *i.e* the backstress α does not evolve. However, the stress state is such that the deviatoric stress progressively moves to the opposite point of the yield surface, $(\sigma - \alpha)$ becomes negative. This change of sign implies that H^p jumps from its minimum value (cf. Eq. 51) to its

maximum one:

$$H_3^p = H_{\max}^p = \sqrt{\frac{2}{3}}\,(h_k + \eta_k\,\alpha_{\max}). \tag{52}$$

Then, between points 3 and 4, the plastic deformation regime restarts in compression while the center of the yield surface is still shifted in the positive σ_1-direction (due to the previous plastic traction). This case corresponds to the one displayed in Fig. 24a. The stress state tends to move the center of the yield surface in the σ_1-reverse direction and the recovery force always tends to bring it back at the origin, both of them act thus in the same direction in this case. The non-lineardynamic recovery term has therefore the effect of speeding up the motion of the yield surface and this effect diminishes as the center of the yield surface approaches the origin. During this process the generalized plastic modulus decreases from $H_{\max}^p$ to $H_4^p = H_1^p = \sqrt{2/3}\,h_k$.

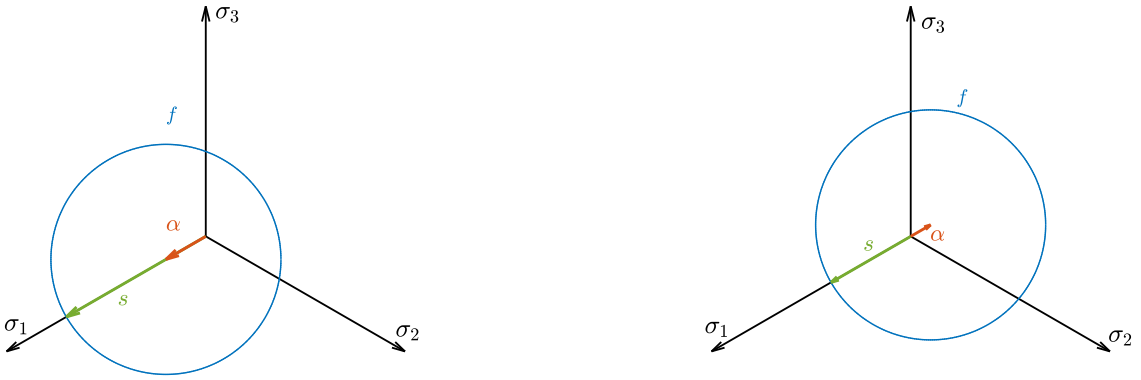

(a) Yield surface shifted in σ_1-direction.

(b) Yield surface shifted in σ_1-reverse direction.

Figure 24: Representation of the backstress α and the deviatoric stress s in *Haigh Westergaard coordinate system* for traction loading.

Between points 4 and 5, the plastic compression continues but with the center of the yield surface shifted behind the plane $O\sigma_2\sigma_3$ (case of Fig. 25b), α becomes negative. As long as the compression loading rises, the center of the yield criterion is shifted further in the σ_1-reverse direction so that α continues to decrease. Therefore, H^p decreases to the same minimum value as in the traction regime (Eq. 51) because the loading cycle is symmetric.

Finally, the material is elastically unloaded between points 5 and 6 with the same consequences as three paragraphs above : $H_6^p = H_{\max}^p$. At the beginning of the plastic traction of the second loading cycle (between points 6 and 7), $(\sigma - \alpha)$ is again positive, the center of the yield surface is brought back in the σ_1-positive direction, $|\alpha|$ decreases. This corresponds to the case of Fig. 24b. At the end $H_7^p = H_1^p$ and all the described cycle restarts.

As a conclusion, the generalized plastic modulus always decreases during plastic deformation. This important result will be observed on the $\bar{\sigma} - \bar{\varepsilon}^p$ evolution curves in the next sections. It has also been shown that the effect of the recovery force sometimes re-enforces the driving effect and is sometimes against it, but is always proportional to

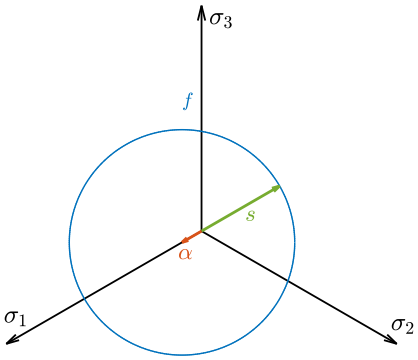

(a) Yield surface shifted in σ_1-direction.

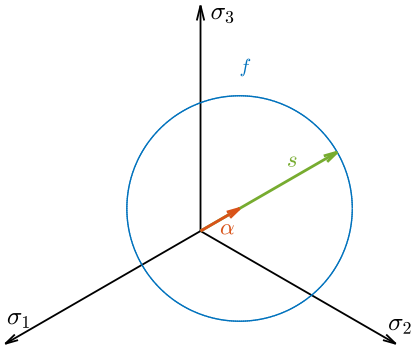

(b) Yield surface shifted in σ_1-reverse direction.

Figure 25: Representation of the backstress α and the deviatoric stress s in *Haigh Westergaard coordinate system* for compressive loading.

the distance between the center of the yield criterion and the origin.

In conclusion, the effect of the dynamic recovery force and the influence of the parameter η_k have been qualitatively discussed and the limit case $\eta_k = 400$ has been identified. Now, the analysis will be split up in three different hardening laws. For each of them, the evolution of the stresses, strains and yield surface will be analyzed. A particular attention will be accorded to the generalized plastic modulus H^p. For all the following discussions, the recovery parameter will be fixed to $\eta_k = 250$. The influence of the maximum traction $t_{\max}$ will also be analyzed, all the graphs will be displayed for $t_{\max}$ =275, 300 and 320 MPa. Larger values would not be compatible with the choice $\eta_k = 250$ as the asymptotic value of the backstress is $\alpha^u = 120$ MPa.

5 Non-linear kinematic hardening

The model used to described non-linear kinematic hardening is the *Armstrong-Frederick's* model, already presented in the introduction of the Section 4. The evolution of the backstress is thus given by Eq. 31. It is obvious that, if the amplitude of the loading increases, the plastic deformation increases. It is confirmed by Fig. 26.

The larger $t_{\max}$, the larger the plastic strain at each loading. For the case $t_{\max} = 320$ MPa, a very fast increase in $\bar{\varepsilon}^p$ at the end of each plastic loading regime can be observed. It can be explained from Eq. 53. Just before the stress σ_{11} reaches its maximum, the backstress is also near its asymptotic value so that the recovery force is almost equal to the driving effect. The additional increase in the backstress needed to compensate the increase of σ is only possible if $\dot{\varepsilon}^p$ is really high.

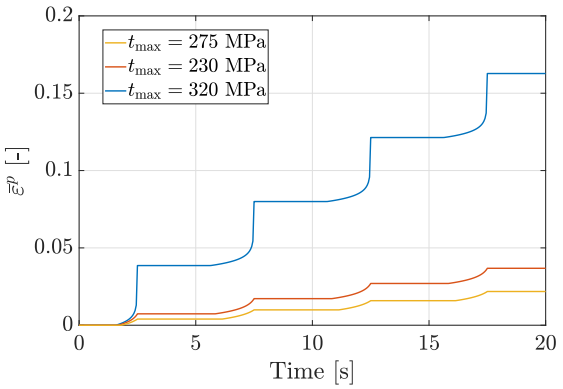

Figure 26: Evolution in time of the equivalent plastic strain in non-linear kinematic hardening for $\eta_k = 250$.

In the purely kinematic hardening model, plasticity only involves the motion of the yield center, *i.e.* the evolution of the backstress. Writing the law $\alpha = \alpha(\dot{\varepsilon}^p)$ is thus really interesting to describe plasticity. Starting from Eq. 31 expressed in the direction of the traction ($i = j = 1$) and taking into account the uni-axial loading, $\alpha_{11} = \frac{2}{3}\alpha$ (Eq. 12) and $\varepsilon^p_{11} = \varepsilon^p$, the equation can be rewritten :

$$\dot{\alpha} = h_k \, \dot{\varepsilon}^p - \eta_k \, \dot{\bar{\varepsilon}}^p \, \alpha. \tag{53}$$

As $\dot{\bar{\varepsilon}}^p = |\dot{\varepsilon}^p|$, the traction and compression loading must be separated.

Traction During the traction, as $\dot{\varepsilon}^p > 0$, $\dot{\bar{\varepsilon}}^p = \dot{\varepsilon}^p$. The first order differential equation can thus be written as:

$$\text{Eq. 53} \quad \Rightarrow \quad \frac{\mathrm{d}\alpha}{\mathrm{d}t} = (h_k - \eta_k \, \alpha)\frac{\mathrm{d}\varepsilon^p}{\mathrm{d}t} \quad \Rightarrow \quad \frac{\mathrm{d}\alpha}{\mathrm{d}\varepsilon^p} + \eta_k \, \alpha = h_k. \tag{54}$$

Since the first order differential Eq. 54 is linear, the solution can be decomposed as a sum of the homogeneous and particular solutions of the heterogeneous solution $\alpha = \alpha_h + \alpha_p$.

Homogeneous solution : $\frac{\mathrm{d}\alpha}{\mathrm{d}\varepsilon^p} + \eta_k \, \alpha = 0 \Rightarrow \alpha_h = C \, \exp\{-\eta_k \, \varepsilon^p\}$,

Particular solution : $\frac{\mathrm{d}\alpha}{\mathrm{d}\varepsilon^p} + \eta_k \, \alpha = h_k \Rightarrow \alpha_p = \frac{h_k}{\eta_k}$,

Initial conditions : $\alpha(\varepsilon^p_0) = \alpha_0 \Rightarrow C = \frac{\alpha_0 - h_k/\eta_k}{\exp\{-\eta_k \, \varepsilon^p_0\}}$,

Solution :

$$\alpha(\varepsilon^p) = \alpha_0 \, \exp\{\eta_k \, (\varepsilon^p_0 - \varepsilon^p)\} + \frac{h_k}{\eta_k}\,(1 - \exp\{\eta_k \, (\varepsilon^p_0 - \varepsilon^p)\}). \tag{55}$$

Compression The development is exactly the same, except the fact that during the compression, as $\dot{\varepsilon}^p < 0$, $\dot{\bar{\varepsilon}}^p = -\dot{\varepsilon}^p$.

$$\text{Eq. 53} \quad \Rightarrow \quad \frac{\mathrm{d}\alpha}{\mathrm{d}t} = (h_k + \eta_k\,\alpha)\frac{\mathrm{d}\varepsilon^p}{\mathrm{d}t} \quad \Rightarrow \quad \frac{\mathrm{d}\alpha}{\mathrm{d}\varepsilon^p} - \eta_k\,\alpha = h_k, \tag{56}$$

Homogeneous solution : $\frac{\mathrm{d}\alpha}{\mathrm{d}\varepsilon^p} - \eta_k\,\alpha = 0 \Rightarrow \alpha_h = C\,\exp\{\eta_k\,\varepsilon^p\}$,

Particular solution : $\frac{\mathrm{d}\alpha}{\mathrm{d}\varepsilon^p} - \eta_k\,\alpha = h_k \Rightarrow \alpha_p = -\frac{h_k}{\eta_k}$,

Initial conditions : $\alpha(\varepsilon_0^p) = \alpha_0 \Rightarrow C = \frac{\alpha_0 + h_k/\eta_k}{\exp\{eta_k\,\varepsilon_0^p\}}$,

Solution :

$$\alpha(\varepsilon^p) = \alpha_0\,\exp\{\eta_k\,(\varepsilon^p - \varepsilon_0^p)\} - \frac{h_k}{\eta_k}\,(1 - \exp\{\eta_k\,(\varepsilon^p - \varepsilon_0^p)\}). \tag{57}$$

In the traction regime, the plastic deformation rate is positive, so that $\varepsilon^p > \varepsilon_0^p$, both exponentials of expression Eq. 55 are decreasing. For an increasing deformation, the expression tends to $\alpha^u = h_k/\eta_k$, which is consistent with the result of Section 4.2. Reversely, in the compression regime, the plastic deformation goes down so that $\varepsilon_0^p > \varepsilon^p$, the exponentials of expression Eq. 57 are also decreasing. While the deformation becomes more negative, the equation tends to the opposite value than for traction : $\alpha^u = -h_k/\eta_k$.

The evolution of the backstress can be visualized for different values of the maximum traction in Fig. 27. The behavior of α is well the one described by Eq. 55 and 57 and the non linearity of the model can clearly be observed. The higher the amplitude of the loading, the higher the plastic deformation and the more the center of the yield surface is moving. As predicted, the backstress converges to its asymptotic value $\alpha^u = \pm 120$ MPa when $t_{\max} =$ 320 MPa, i.e. when the maximum prescribed displacement is increased a lot. As explained in the beginning of this section, a very large increase in ε^p is required for this convergence of α.

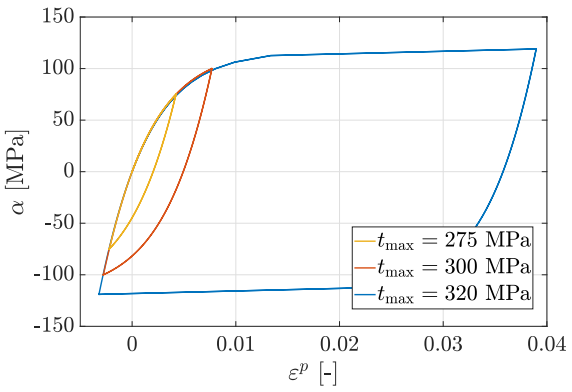

Figure 27: Evolution of the backstress with the plastic strain for non-linearkinematic hardening, $\eta_k = 250$.

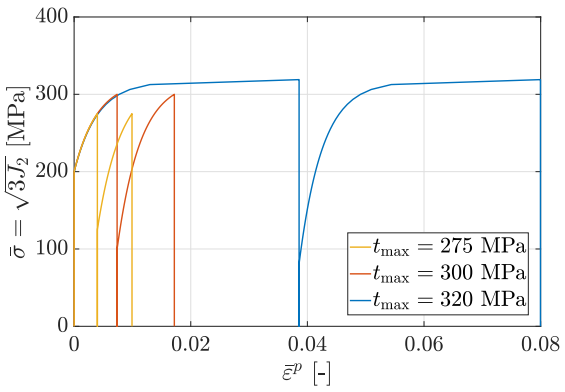

Figure 28: Evolution of the equivalent stress with the equivalent plastic strain for non-linearkinematic hardening, $\eta_k = 250$.

Starting from the consistency condition and using the associated flow rule and the small deformations assumption, it can be shown that

$$\dot{\sigma}_{ij}\dot{\varepsilon}^p_{ij} = \sqrt{\frac{3}{2}}\, H^p\, (\dot{\bar{\varepsilon}}^p)^2 \,. \tag{58}$$

Under uni-axial loading condition, $\dot{\sigma}_{ij}\dot{\varepsilon}^p_{ij}$ reduces to $\dot{\sigma}\dot{\varepsilon}^p$, $\dot{\bar{\varepsilon}}^p = |\dot{\varepsilon}^p|$ and $\bar{\sigma} = |\sigma|$, the last equation can be re-expressed as Eq. 59.

$$\dot{\bar{\sigma}} = \sqrt{\frac{3}{2}}\, H^p\, |\dot{\bar{\varepsilon}}^p| \quad \Rightarrow \quad \frac{\mathrm{d}\bar{\sigma}}{\mathrm{d}\bar{\varepsilon}^p} = \sqrt{\frac{3}{2}}\, H^p = h(\bar{\varepsilon}^p). \tag{59}$$

As a conclusion, the plastic modulus h can be interpreted as the slope of the curve $\bar{\sigma} - \bar{\varepsilon}^p$.

As already discussed in Section 4.3, the general plastic modulus H^p always decreases during plastic deformation : that can effectively be observed in Fig. 28, since the slope of the curve $\bar{\sigma} - \bar{\varepsilon}^p$ is always decreasing. Furthermore, this slope is not modified with the amplitude of the load, only the maximum stress that is reached and the corresponding plastic deformation increase with $t_{\max}$. Moreover, in the stress-strain space, the curve $\sigma - \varepsilon^p$ does not represent a closed cycle.

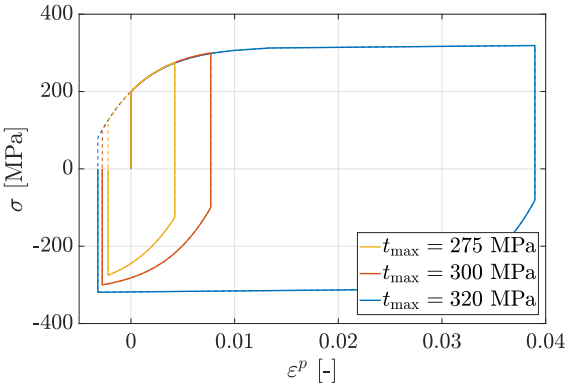

Figure 29: Stress-strain space.

Indeed, at the end of the cycle, it remains a negative permanent plastic deformation due to the latest compression. This curve is nevertheless closed a the beginning of the next cycle (dashed line of Fig. 29).

Finally, it is possible analyze the yield surface in the *Haigh Westergaard's space*. Excepted the evolution of the backstress that is now non-linear, the evolution of the yield surface will be really similar to the linear case (cf. Fig. 10a), it is only a translation of its center. It is possible to define an asymptotic yield surface f', described by the upper bound of the equivalent stress $\sqrt{3\,J_2}$ where $\sqrt{3\,J_2} = \sqrt{\frac{3}{2}\, s_{ij}s_{ij}} = \sqrt{\frac{3}{2}}\|\boldsymbol{s}\|$. Using the triangular inequality, it comes :

$$\begin{aligned}\sqrt{3\,J_2} = \sqrt{\frac{3}{2}}\|\boldsymbol{s}\| = \sqrt{\frac{3}{2}}\|\boldsymbol{s} - \boldsymbol{\alpha} + \boldsymbol{\alpha}\| &\leq \sqrt{\frac{3}{2}}\|\boldsymbol{s} - \boldsymbol{\alpha}\| + \sqrt{\frac{3}{2}}\|\boldsymbol{\alpha}\| \\ &\leq \sqrt{\frac{3}{2}(s_{ij} - \alpha_{ij})(s_{ij} - \alpha_{ij})} + \sqrt{\frac{3}{2}\,\alpha_{ij}\alpha_{ij}}\end{aligned}$$

$$\sqrt{3\,J_2} \leq \bar{\sigma}^{VM} + \bar{\alpha}. \tag{60}$$

In purely kinematic hardening, the upper bound of $\sqrt{3\,J_2}$ is reached when $\bar{\alpha} = \bar{\alpha}^u = h_k/\eta_k$, $\bar{\sigma}^{VM} = \sigma^0_y$ during all the plasticity.

The asymptotic yield surface is therefore given by Eq. 61:

$$f' = \sqrt{3\,J_2} - \left(\sigma_y^0 + \frac{h_k}{\eta_k}\right) \leq 0. \qquad (61)$$

In Fig. 30, the yield surface is displayed at the maximum traction for different values of $t_{\max}$ and at the maximum compression for $t_{\max} = 320$ MPa. It can be seen that the stress state (denoted by the dot) reaches the asymptotic yield surface for both maximum traction and compression. It is not the case for lower amplitude of the loading.

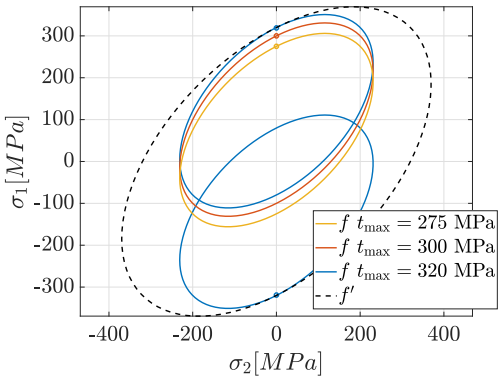

Figure 30: Representation of the asymptotic yield surface in the case of a non-linear kinematic hardening.

5.1 Plastic dissipation

When there is plasticity, some energy is dissipated. About 5 to 10 % of this dissipated energy is used in order to rearrange the atoms and the dislocations, and 90 to 95% is dissipated into heat.

The plastic dissipation is given by Eq. 27. It can be rewritten as:

$$\mathbb{D} = \bar{\sigma}\dot{\bar{\varepsilon}}^p = \bar{\sigma}\sqrt{\frac{2}{3}}\lambda. \qquad (62)$$

It is possible to compare the linear kinematic hardening and the non-linear kinematic hardening in terms of the plastic dissipation.

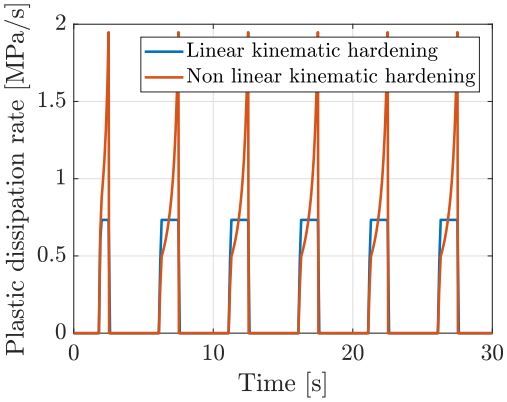

Figure 31: Evolution in time of plastic dissipation rate with $t_{max} = 275$ MPa and $\eta_k = 250$.

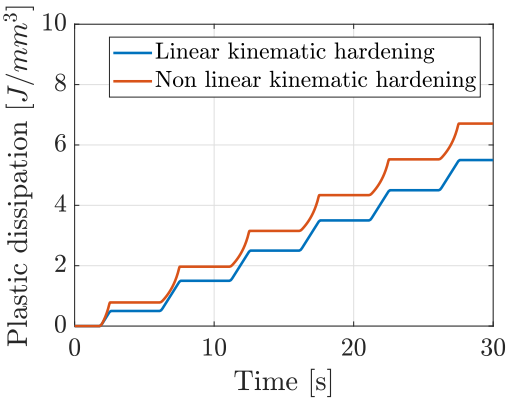

Figure 32: Evolution in time of plastic dissipation with $t_{max} = 275$ MPa and $\eta_k = 250$.

As it can be seen in Fig. 31 and Fig. 32, the plastic dissipation is bigger in the case of a non-linear kinematic hardening. The expressions of λ (the way the analytical expression of λ is computed in the non-linear case will be explained later in the text) for

the two cases are:

$$\lambda_{\text{linear kinematic}} = \frac{N_{kl} D_{kl}}{1 + \frac{h_k}{3G}}, \tag{63}$$

$$\lambda_{\text{non-linear kinematic}} = \frac{N_{kl} D_{kl}}{1 + \frac{h_k}{3G} - \frac{\eta_k}{\sqrt{6}G} \alpha_{ij} N_{ij}}. \tag{64}$$

Therefore, it can be noted that due to the lower denominator of $\lambda_{\text{non-linear kinematic}}$, this one is bigger than $\lambda_{\text{linear kinematic}}$. That is why the plastic dissipation in the non-linear case is much bigger than in the linear case.

It can also be observed that the plastic dissipation rate is constant for the linear case, while it evolves exponentially for the non-linear case. Indeed, $\lambda_{\text{non-linear kinematic}}$ is not constant in time, as it will be discussed in the following section.

6 Mixed hardening

6.1 Non-linear kinematic hardening combined with linear isotropic hardening

In this section, the evolution of the backstress of *Armstrong-Frederic's* model (cf. Eq. 31) will be combined with the evolution of the yield stress of the linear isotropic hardening model (cf. Eq. 8). In this case, the yield criterion is therefore written as:

$$f = \bar{\sigma} - \sigma_y(\bar{\varepsilon}^p) = \sqrt{\frac{3}{2}(s_{ij} - \alpha_{ij})(s_{ij} - \alpha_{ij})} - (\sigma_y^0 + h_i\, \bar{\varepsilon}^p) \leq 0. \tag{65}$$

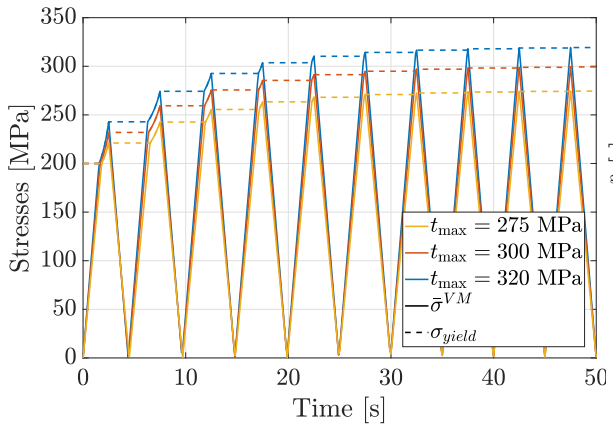

Figure 33: Evolution in time of stresses for $\eta_k = 250$ and different values of $t_{\max}$.

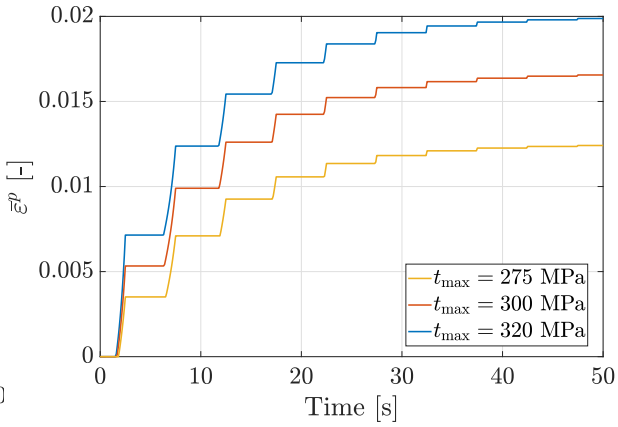

Figure 34: Evolution in time of the equivalent plastic strains for $\eta_k = 250$ and different values of $t_{\max}$.

As the model used to described kinematic hardening has not changed, the evolution of the backstress as a function of the plastic deformation derived in previous section is still valid. However, as the yield stress increases at each loading cycle, the plastic deformation decreases. It is why the backstress decreases trough cycles.

The yield stress is only affected by the isotropic part of the hardening model. Since the isotropic hardening model used in this section is linear, the evolution of the yield stress is linear with the effective plastic strain. However, one can notice that the evolution of the yield stress with time is non-linear when analyzing Fig. 33. From a mathematical point of view, it can be explained with the expression of the plastic multiplier λ. Indeed, the time evolution of σ_y is given by

$$\dot{\sigma_y} = h_i \dot{\bar{\varepsilon}}^p = \sqrt{\frac{2}{3}} h_i \lambda. \tag{66}$$

The general analytical expression of the plastic multiplier is

$$\lambda = \frac{\frac{\partial f}{\partial \sigma_{ij}} \mathbb{H}_{ijkl} D_{kl}}{\frac{\partial f}{\partial \sigma_{ij}} \mathbb{H}_{ijkl} N_{kl} - \frac{\partial f}{\partial \boldsymbol{q}^{(v)}} * \boldsymbol{r}^{(v)}}. \tag{67}$$

The expression Eq. 67 can be drastically simplified thanks to the following considerations :

1. Only the deviatoric part of the stress influences plasticity so that

$$\frac{\partial f}{\partial \sigma_{ij}} = \frac{\partial f}{\partial s_{ij}} = \sqrt{\frac{3}{2}} \frac{s_{ij} - \alpha_{ij}}{\sqrt{(s_{ij} - \alpha_{ij})(s_{ij} - \alpha_{ij})}}. \tag{68}$$

2. Using the associative flow rule, the direction of the plastic flow is given by

$$N_{ij} = \frac{s_{ij} - \alpha_{ij}}{\sqrt{(s_{ij} - \alpha_{ij})(s_{ij} - \alpha_{ij})}} \xrightarrow{\text{Eq. 68}} \quad \frac{\partial f}{\partial \sigma_{ij}} = \sqrt{\frac{3}{2}} N_{ij}. \tag{69}$$

3. As the Hooke's tensor is given by Eq. 70 where K and G are respectively the bulk modulus and the shear modulus, and using the fact that $\boldsymbol{N}$ is deviatoric ($\text{tr}(\boldsymbol{N}) = N_{kk} = 0$), it comes :

$$\mathbb{H}_{ijkl} = K \delta_{ij} \delta_{kl} + G(\delta_{ik}\delta_{jl} + \delta_{il}\delta_{kj} - \frac{2}{3}\delta_{ij}\delta_{kl}), \tag{70}$$

$$\mathbb{H}_{ijkl}\, N_{kl} = 2G\, N_{ij}. \tag{71}$$

4. The internal parameters needed to describe mixed hardening are α_{ij} and $\bar{\varepsilon}^p$. The

expressions of the functions r given in Section 4.1. It allows to write:

$$\begin{aligned}\frac{\partial f}{\partial \boldsymbol{q}^{(v)}} * \boldsymbol{r}^{(v)} &= \frac{\partial f}{\partial \alpha_{ij}} r(\boldsymbol{\sigma}, \alpha_{ij}) + \frac{\partial f}{\partial \bar{\varepsilon}^p} r(\boldsymbol{\sigma}, \bar{\varepsilon}^p) \\ &= -\sqrt{\frac{3}{2}} \underbrace{\frac{s_{ij} - \alpha_{ij}}{\sqrt{(s_{ij} - \alpha_{ij})(s_{ij} - \alpha_{ij})}}}_{=N_{ij}} \left(\frac{2}{3} h_k \, N_{ij} - \sqrt{\frac{2}{3}} \eta_k \, \alpha_{ij} \right) - \sqrt{\frac{2}{3}} h_i \\ &= -\sqrt{\frac{2}{3}} h_k \underbrace{N_{ij} N_{ij}}_{=1} \sqrt{\frac{2}{3}} h_i + \eta_k \, \alpha_{ij} N_{ij} \\ &= -\sqrt{\frac{2}{3}} h + \eta_k \, \alpha_{ij} N_{ij}. \end{aligned} \tag{72}$$

Therefore, the denominator of λ becomes

$$\frac{\partial f}{\partial \sigma_{ij}} \mathbb{H}_{ijkl} N_{kl} - \frac{\partial f}{\partial \boldsymbol{q}^{(v)}} * \boldsymbol{r}^{(v)} = \sqrt{\frac{3}{2}} 2G \underbrace{N_{ij} N_{ij}}_{=1} + \sqrt{\frac{2}{3}} h - \eta_k \, \alpha_{ij} N_{ij}. \tag{73}$$

5. Using the Eq. 69 and 71, the numerator of λ becomes

$$\frac{\partial f}{\partial \sigma_{ij}} \mathbb{H}_{ijkl} D_{kl} = \sqrt{\frac{3}{2}} 2G \, N_{kl} D_{kl}. \tag{74}$$

Finally the expression of λ is

$$\lambda = \frac{N_{kl} D_{kl}}{1 + \frac{h}{3G} - \frac{\eta_k}{\sqrt{6}G} \alpha_{ij} \, N_{ij}}. \tag{75}$$

As a conclusion, the expression of λ depends in this case on the backstress which evolves in time and depends on the stress state. Therefore $\dot{\sigma}_y$ is not a constant so that σ_y is non-linear in time.

In this case, it is expected that while increasing the applied load, the yield stress will rise without any upper bound to finally reach this $t_{\max}$ after several cycles. Therefore, it is not useful to consider the asymptotic value of the yield stress because its value depends on $t_{\max}$ and can, theoretically, increase infinitely with $t_{\max}$. The equivalent stress $\sqrt{3J_2}$ is thus not bounded in this case and the asymptotic yield surface f' is not defined. Moreover, it can be noticed that the equivalent backstress always tends to zero with increasing the number of cycles. Indeed, due to the fact that the yield surface will be expanded with the increasing value of σ_y, the plastic regime is reduced, the yield surface is so expanded that all the loading/unloading tends to take place in the elastic regime. This explains why the backstress tends to zero (Fig. 35). Also, the decrease of the plastic regime can be noted by analyzing the vertical steps becoming smaller and smaller in Fig. 34.

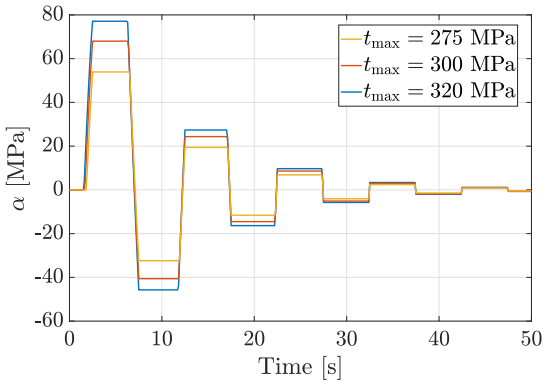

Figure 35: Evolution in time of the backstress for non-linear kinematic hardening combined with a linear isotropic hardening, $\eta_k = 250$.

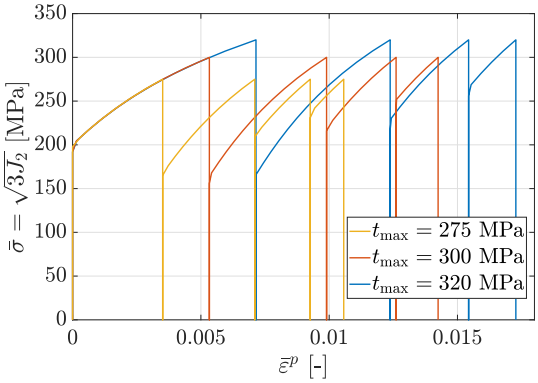

Figure 36: Evolution of equivalent stress with the equivalent plastic strain for a non-linear kinematic hardening combined with linear isotropic hardening, $\eta_k = 250$.

In the case of non-linear kinematic hardening combined with linear isotropic hardening, the generalized plastic modulus has the form of Eq. 76. It is exactly the same form as Eq. 50 with an additional constant term due to isotropic hardening. The slope of the curve $\bar{\sigma} - \bar{\varepsilon}^p$ will thus be higher but with exactly the same behavior as for the previous case: the slope decreases during the plasticity. This can be observed in Fig. 36.

$$H^p = \sqrt{\frac{2}{3}}\, h_k - \sqrt{\frac{2}{3}}\, \eta_k\, \alpha \frac{(\sigma - \alpha)}{|\sigma - \alpha|} + \sqrt{\frac{2}{3}}\, h_i. \tag{76}$$

6.2 Non-linear kinematic hardening combined with non-linear isotropic hardening

In this section, non-linear kinematic hardening described by *Armstrong Frederick's* model (cf. Eq. 31) will be combined with non-linear isotropic hardening described by *Voce's* saturated law. The evolution of the yield stress is given by

$$\sigma_y = \sigma_y^\infty - (\sigma_y^\infty - \sigma_y^0) \exp\left\{ - \frac{h_i\, \bar{\varepsilon}^p}{\sigma_y^\infty - \sigma_y^0} \right\}. \tag{77}$$

As the number of cycles increases, the material hardens more and more, the yield stress is thus increasing. Due to the fact that σ_y is higher and higher, the time lapse over which plastic regime takes place decreases. In fact, the yield surface is going to be expanded more and more, and this leads to quasi elastic processes. This is why the backstress decreases, and this gives rise to an equivalent backstress tending to zero over the loading/unloading cycles. The decrease of the plastic regime time lapse can also be noted by looking at Fig. 38. In fact, in the graphical representation of the equivalent plastic strain over time, the vertical steps are becoming lower and lower when evolving through the cycles. This decrease is thus larger for a large number of cycles. These observations are valid for $t_{max} = 275$ MPa as it can be observed for the yellow curve in Fig. 38, Fig. 39 and Fig. 40.

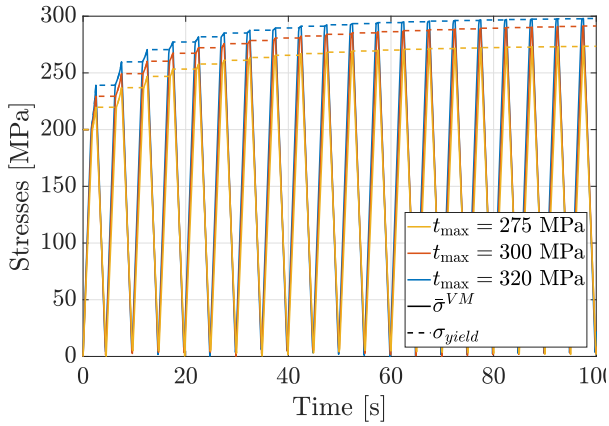

Figure 37: Evolution of stresses with time for $\eta_k = 250$ and different values of $t_{\max}$.

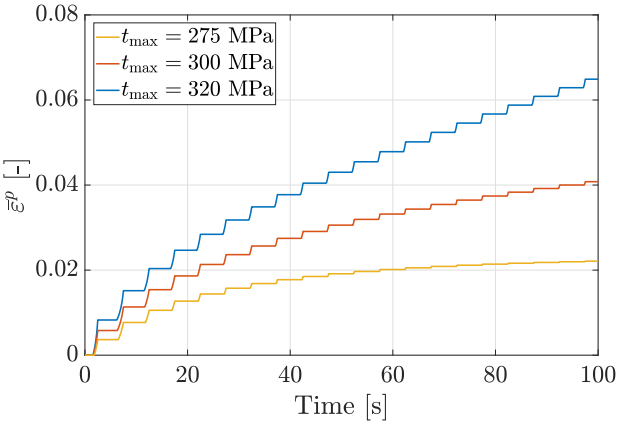

Figure 38: Evolution of the equivalent plastic strains for $\eta_k = 250$ and different values of $t_{\max}$.

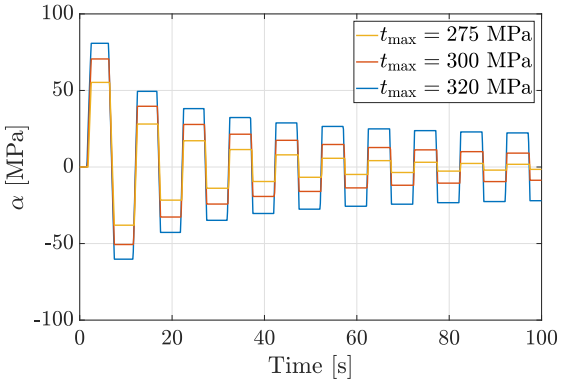

Figure 39: Evolution in time of the backstress for non-linear kinematic hardening with non-linear isotropic hardening, $\eta_k = 250$.

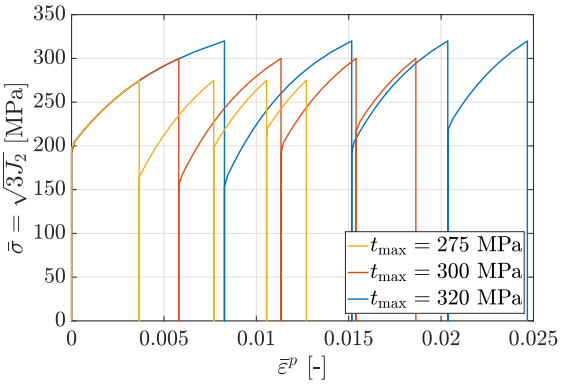

Figure 40: Evolution of the equivalent stress with the equivalent plastic strain for non-linear kinematic hardening with non-linear isotropic hardening, $\eta_k = 250$.

In order to deduce the asymptotic value of σ_y, its derivative with respect to time must be equal to 0. Considering the expression of $\sigma_y(\bar{\varepsilon}^p)$ given by Eq. 77, it comes:

$$\dot{\sigma_y} = \frac{\partial \sigma_y}{\partial \bar{\varepsilon}^p} \dot{\bar{\varepsilon}}^p = \dot{\bar{\varepsilon}}^p \exp\left\{\frac{-h_i \bar{\varepsilon}^p}{\sigma_y^\infty - \sigma_y^0}\right\}. \tag{78}$$

This derivative is equal to 0 for $\bar{\varepsilon}^p$ tending to infinity. Therefore, the asymptotic value of the yield stress is given by

$$\sigma_y^u = \lim_{\bar{\varepsilon}^p \to \infty} \sigma_y(\bar{\varepsilon}^p) = \sigma_y^\infty = 300 \text{ MPa}. \tag{79}$$

For $t_{\max} = 320$ MPa, it can be noticed that the equivalent plastic strain still increases with non negligible steps at each cycle of the loading. At the same time, the backstress is first decreasing in absolute value but its amplitude of oscillations does not tend to

zero. In fact, $t_{\max}$ is greater than the asymptotic value of the yield stress. When σ_y has reached this value, the yield surface cannot expand anymore and the hardening becomes purely kinematic. The yield surface is only translated. The backstress oscillates with an amplitude of $t_{\max} - \sigma_y^\infty$, as it can be seen for the blue curve in Fig. 40.

For the particular case of $t_{\max}$ exactly equal to $\sigma_y^u = 300$ MPa, almost the same observations could be made as for the case $t_{\max} = 275$ MPa. However the convergence is very slow and can barely be observed after 10 cycles.

The very slow convergence of the yield stress can be explained by the fact that the backstress evolves much faster with the plastic strain than the yield stress. Indeed, σ_y and α both evolve with a decreasing exponential of the plastic strain (cf. resp. Eq. 77 and Eq. 55), but with different constants : $\frac{h_i}{\sigma_y^\infty - \sigma_y^0} = 60$ for σ_y and $\eta_k = 250$ for α. The yield surface moves faster than it expands, which is coherent with the fact that the model is mainly kinematic ($\theta^* = 0.2$).

In the same way as for purely kinematic hardening model, the asymptotic yield stress can be deduced from the upper bound of $\bar{\sigma} = \sqrt{3\,J_2}$, *i.e.* when the equivalent backstress $\bar{\alpha}$ and the yield stress σ_y reach both their asymptotic value. This upper bound of $\sqrt{3\,J_2}$ is therefore $300 + 24000/250 = 396$ MPa.

$$f' = \sqrt{3J_2} - (\sigma_y^\infty + \frac{h_k}{\eta_k}) = 0. \tag{80}$$

Note that if a traction of $t_{\max} = 396$ MPa was applied, as the backstress is limited to 96 MPa, the yield stress would converge to its asymptotic value in one cycle (and the yield surface would reach its asymptotic configuration as it can be seen for the black dashed line in Fig. 41). As mentioned, it can be seen in Fig. 41 that for $t_{\max} = 320$ MPa, the yield surface has a lager size during the 10^{th} cycle than during the first one, but moves less.

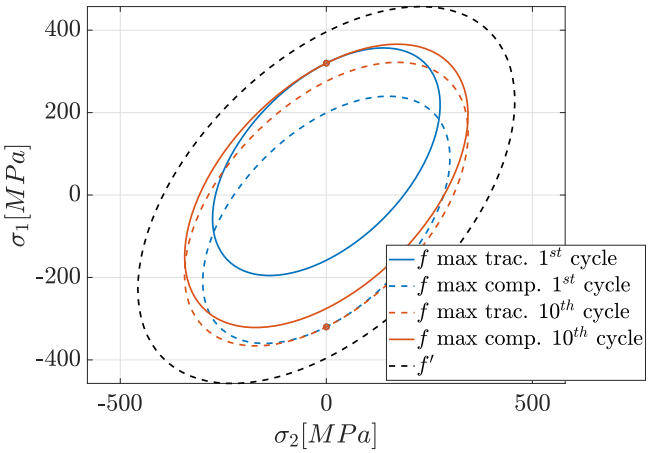

Figure 41: Representation of the asymptotic yield surface for $t_{\max} = 320$ MPa.

In this case, the generalized plastic modulus is given by

$$H^p = \sqrt{\frac{2}{3}}h_k - \eta_k\sqrt{\frac{2}{3}}\frac{(\sigma-\alpha)}{|\sigma-\alpha|}\alpha + \sqrt{\frac{2}{3}}h_i \exp\left\{\frac{-h_i\bar{\varepsilon}^p}{\sigma_y^\infty - \sigma_y^0}\right\}. \tag{81}$$

It can be observed from this equation that the non-linear isotropic term tends to decrease H^p when $\bar{\varepsilon}^p$ increases. The reduction in the slope of the curve $\bar{\sigma} - \bar{\varepsilon}^p$ during plasticity explained in Section 5 is therefore reinforced. It can be seen in Fig. 40.

Part III

Elasto-viscoplastic behavior

After all this first study, an important parameter can be added to the current analysis: the viscosity η. Indeed, it is now possible to consider the elasto-viscoplatic behavior of the cube subjected to linear hardening laws. In this particular case, the yield function f still exists but in the inelastic regime, this one can now be zero or positive. As a consequence, the flow parameter value (λ) which is defined by the irreversible deformation $\boldsymbol{D}^{vp} = \lambda \boldsymbol{N}$ can not be determined by the consistency condition anymore. The elasto-viscoplastic behavior requires an hypothesis on the form of λ. A well known assumption is the *Perzyna's* model:

$$\lambda = \sqrt{\frac{3}{2}} \left\langle \frac{\bar{\sigma} - \sigma_y}{\eta (\bar{\varepsilon}^{vp})^n} \right\rangle^{\frac{1}{m}}, \tag{82}$$

where $\frac{1}{n}$ and $\frac{1}{m}$ are respectively the hardening and viscosity exponents, η is the viscosity parameter and $\langle x \rangle = \frac{1}{2}(x + |x|)$ are the *Mc. Auley* brackets.

The overstress which represents the distance from the stress state to the yield surface in the *Haigh Westergaard's space* can also be computed since the effective stress can go outside of the yield criterion during plasticity ($f \geq 0$ is possible):

$$d = \langle \bar{\sigma} - \sigma_y \rangle. \tag{83}$$

In this study, the values for m and n are respectively 1 and 0 so that the effective visco-plastic strain does not directly influence λ.

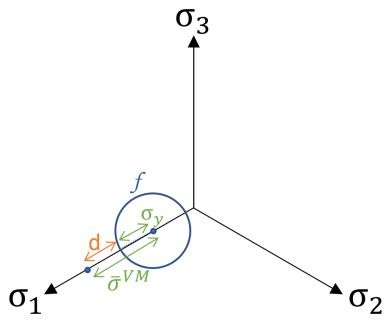

Figure 42: Definition of the overstress.

As a consequence, the effective visco-plastic strain rate can be computed by

$$\dot{\bar{\varepsilon}}^{vp} = \sqrt{\frac{2}{3} \boldsymbol{D}^{vp} : \boldsymbol{D}^{vp}} = \sqrt{\frac{2}{3}} \lambda = \left\langle \frac{\bar{\sigma} - \sigma_y}{\eta} \right\rangle \tag{84}$$

and the linear hardening laws are described by the following variables:

$$\dot{\sigma}_y = h_i \dot{\bar{\varepsilon}}^{vp} = h_i \left\langle \frac{\bar{\sigma} - \sigma_y}{\eta} \right\rangle, \tag{85}$$

$$\dot{\boldsymbol{\alpha}} = \frac{2}{3} h_k \lambda \boldsymbol{N} = \sqrt{\frac{2}{3}} h_k \boldsymbol{N} \left\langle \frac{\bar{\sigma} - \sigma_y}{\eta} \right\rangle, \tag{86}$$

where $\dot{\sigma}_y$ describes the evolution of the yield stress. Note that in the two previous equations, the hardening coefficients are linked, as already mentioned in Part I, by $h =$

$h_i + h_k$. The previous consistency equation being not correct anymore, a new one can be extended and this one must be verified for any visco-plastic materials:

$$\bar{f} = \bar{\sigma} - \sigma_y - \eta\dot{\bar{\varepsilon}}^{vp} = 0. \tag{87}$$

One can easily see that the term $\eta\dot{\bar{\varepsilon}}^{vp}$ must have the same units as a stress [MPa] in order to get the Eq. 87 consistent. The equivalent visco-plastic strain rate being measured in [s^{-1}], the units of η are imposed to [MPa.s].

One can notice an important thing about the *Mac Auley* brackets : if the argument is negative, the whole value vanishes. As a consequence, when $\bar{\sigma} < \sigma_y$, $\lambda = 0$ and the elastic regime is regained. Since the intensity of the plastic flow is zero, all the other values $\dot{\bar{\varepsilon}}^{vp}$, $\dot{\sigma_y}$ and $\dot{\boldsymbol{\alpha}}$ vanishes. Therefore, for the first entry in plasticity, the cube with a visco-plastic behavior will enter into plasticity at the same time than in the simple elasto-plastic case.

7 Influence of the viscous parameter

It is obvious that the value of the viscous parameter η will play an important role in the behavior of the cube.

A first effect to notice is the influence of η on the behavior of the equivalent visco-plastic strain $\bar{\varepsilon}^{vp}$ and the yield stress σ_y. According to Eq. 84 and 85, when η increases, $\dot{\bar{\varepsilon}}^{vp}$ and $\dot{\sigma_y}$ decrease. Thus, $\bar{\varepsilon}^{vp}$ and σ_y present a lower slope (cf. Fig. 43a and 43b). It means that in a same time, they can grow less. These results were expected because if there is more viscosity, it is more difficult to expand the yield surface. One can note that these results are presented in the linear isotropic hardening case but they are also valid in the kinematic and mixed cases.

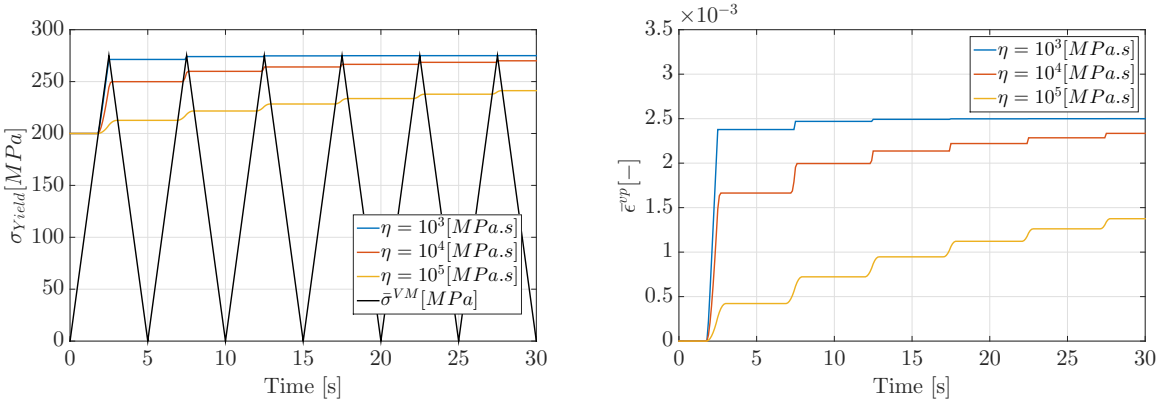

(a) Evolution in time of the yield stress.

(b) Evolution in time of the strains.

Figure 43: Linear isotropic hardening model in a plane stress state for different values of η.

The behaviors of $\bar{\varepsilon}^{vp}$ and σ_y can also explain the influence of η on the overstress (cf. Fig 44). The time-evolution of $\bar{\sigma}$ is independent of the value of η since it is expressed as $\bar{\sigma} = \sqrt{\frac{3}{2} s_{ij} s_{ij}}$ (represented in black in Fig 43a) and, as it has just been said, the value of σ_y is lower for higher η. This is why d increases when η increases. It can be seen as the fact that the yield surface is less extended so the distance to the stress state is larger.

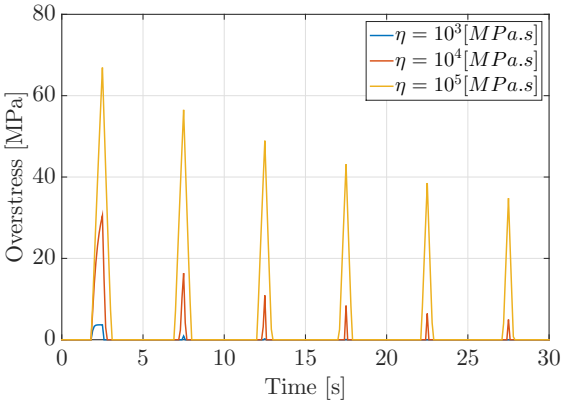

Figure 44: Evolution in time of the overstresses with a linear isotropic hardening model in a plane stress state for different values of η.

In the mixed hardening model, the influence of the viscosity on the effective strain, on the yield stress and on the overstress is very similar to what has been obtained for the isotropic case. They are not displayed here to avoid redundancy.

However, there is now the equivalent backstress that is non-zero anymore. Indeed, Eq. 86 shows that, in plasticity, if η increases $\dot{\alpha}$ decreases. As a consequence, the slope of the increasing $\bar{\alpha}$ is smaller and therefore, for a same duration of time spent in plasticity, the $\bar{\alpha}$ will be smaller. Therefore, if the α_{ij} are smaller, the $\bar{\sigma}^{VM}$ is bigger and then the distance between the yield surface and the effective stress increases with η.

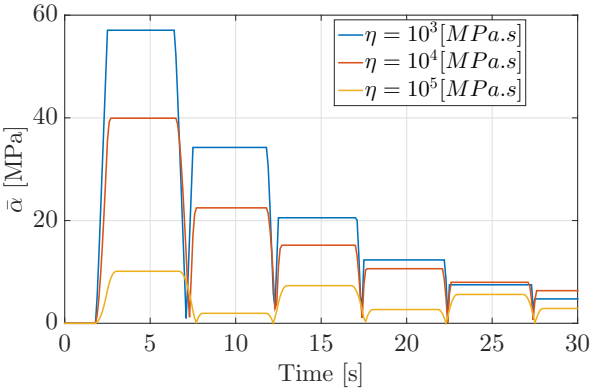

Figure 45: Evolution in time of $\bar{\alpha}$ with a linear mixed hardening model in a plane stress state for different values of η.

Several values of the viscous parameter have been here studied and the limit cases will be studied in the next section. For further analysis, only the case $\eta = 10^5$ MPa.s will be considered in order to clearly see the effect of viscosity.

7.1 Limit cases

In this part, two limit values of η will be presented in order to retrieve well known cases.

The case $\eta = \infty$ is first analyzed. Thanks to Eq. 84, one can see that if $\eta = \infty$, the value of $\dot{\bar{\varepsilon}}^{vp}$ tends to 0 (cf. Fig. 46a). This means that there is no equivalent plastic strain. Thus, the yield surface is not translated nor expanded. This corresponds thus to a perfectly elastic regime. This can also be seen in the stress strain space (cf. Fig. 46b)

where the path is reduced to a single line. These two graphs have been plotted with $\eta = 10^9$ MPa.s which has been supposed sufficiently high to consider it takes an infinite value. Moreover, whatever the model of hardening used, the results are the same.

The second limit case $\eta = 0$ is now considered. The consistency equation (cf. Eq. 87) becomes:

$$\bar{f} = \bar{\sigma} - \sigma_y = 0. \tag{88}$$

Therefore, the overstress in plasticity is given by $d = \bar{\sigma} - \sigma_y = 0$ and so, the numerator of $\dot{\bar{\varepsilon}}^{vp}$ is equal to zero too. The standard Von Mises yield criterion for plasticity is recovered ($\bar{f} \equiv f$) and it is thus the classical elasto-plastic case studied before.

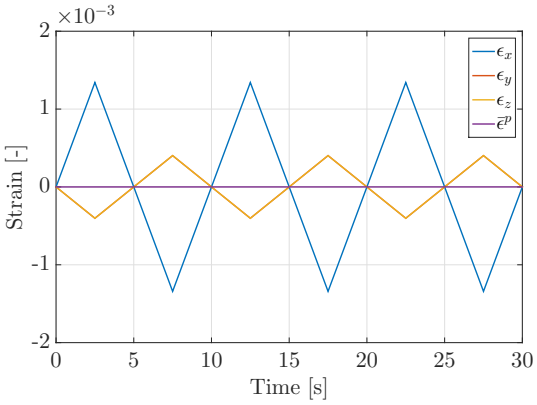

(a) Evolution in time of the strains.

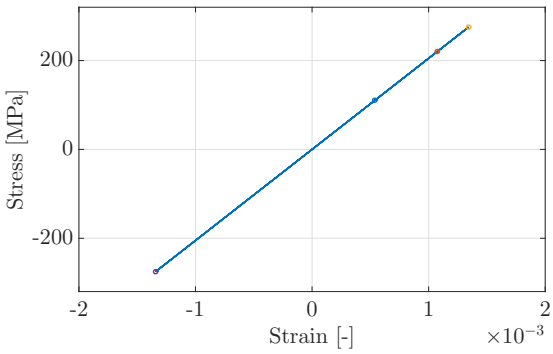

(b) Strain-stress space.

Figure 46: Any hardening model in a plane stress with $\eta = 10^9$ MPa.s.

7.2 Time dependency

Another really important point to mention in the elasto-viscoplastic behavior is the fact that the stresses depend on the loading rate and so do the maximum overstress.

Indeed, this is shown in Fig. 47 for which the load is applied in $1s$, $2.5s$ and $5s$ and then is kept constant in the linear isotropic case. One can note that the higher the loading speed, the higher maximum overstress. This effect is also present in the case of kinematic and mixed hardening laws. This is explained by two microscopic phenomena: the sliding of the grain boundaries and the motion and multiplication of dislocations that are due to the presence of viscosity.

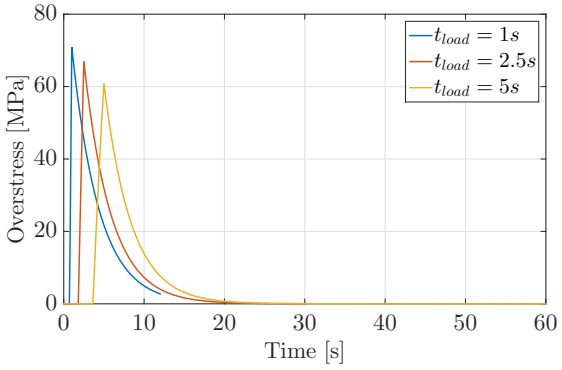

Figure 47: Influence of the loading speed on $d_{\max}$.

8 General cases

In this section, the three models: perfectly plastic, isotropic and mixed hardening will be studied for different types of loading curve considering $\eta = 10^5\ MPa \cdot s$.

8.1 Perfectly plastic model

For a model with no hardening at all, $h = h_k = h_i = 0$. By replacing this in the Eq. 85, it gives $\dot{\sigma}_y = 0$ and σ_y is thus constant and equal to the yield stress of the virgin material. Since σ_y and η are both constant, $\dot{\bar{\varepsilon}}^{vp}$ depends only on $\bar{\sigma}$ (cf. Eq. 84).

In this case, the load is applied linearly from 0 to $t_{\max}$ and is then kept constant for a long duration time (cf. Fig. 48a). Thus, when the load is constant in plasticity, $\bar{\sigma} = \sqrt{\frac{3}{2}s_{ij}s_{ij}} = |\sigma_{11}|$ is constant. The value of $\dot{\bar{\varepsilon}}^{vp}$ is thus constant. An integration over time allows thus to see that $\bar{\varepsilon}^{vp}$ has first an increasing slope and then passes rapidly to a linear evolution after 2.5s (cf. Fig. 48b); the value of this slope is inversely proportional to η. One can observe that $\bar{\varepsilon}^{vp}$ tends to infinity for a long time and the assumption of small deformations is therefore not valid anymore.

One can note that before the entry in plasticity (i.e. when $\bar{\sigma} < \sigma_{yield}$), the numerator of the Eq. 84 is smaller than zero. Therefore, $\dot{\bar{\varepsilon}}^{vp}$ is zero and there is no equivalent strain in the elastic regime as already mentioned.

One important thing to notice is the fact that this time, even if $\sigma_{\max}$ is bigger than σ_y^0, the software Metafor compiles and returns a solution. Indeed, in the visco-elastoplastic domain, the yield function f can be positive as it was not the case without viscosity. In fact, by imposing the *Perzyna's* law, this is the extended consistency equation that is now taken into account and $\bar{\sigma}$ can be bigger than σ_y.

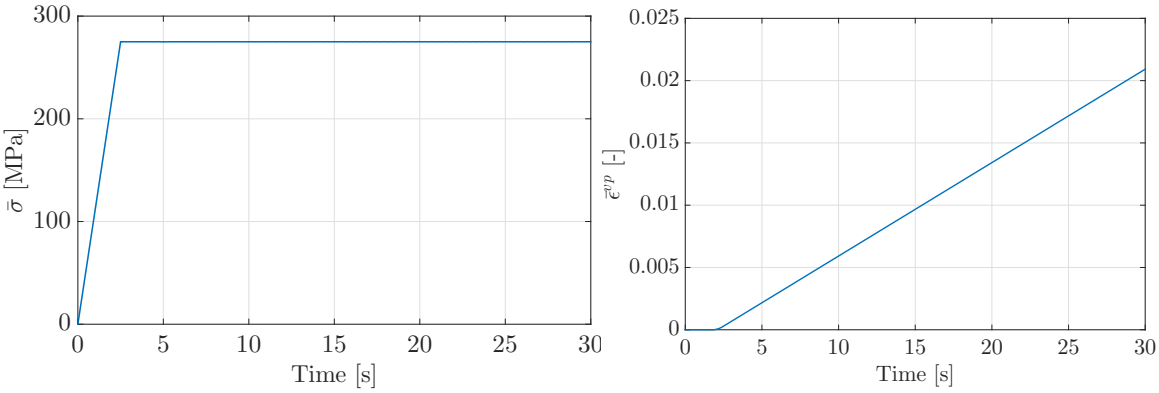

(a) Evolution in time of the stress.

(b) Evolution in time of the strain.

Figure 48: Elasto-viscoplastic behavior without hardening with $\eta = 10^5$ MPa.s for the imposed load kept constant at $t_{\max}$.

8.2 Isotropic hardening model

In the isotropic hardening model, $h = h_i$ and thus $h_k = 0$. As a consequence, the backstresses are zeros; however, the yield stress is not constant anymore. Indeed, Eq. 85

can be integrated and knowing that $\sigma_y = \sigma_y^0$ before the first entry into plasticity, it leads to:

$$\sigma_y = h\bar{\varepsilon}^{vp} + \sigma_y^0. \tag{89}$$

This is represented in Fig. 49a for a load kept constant at $\sigma_{\max} = t_{\max}$ for an infinitely long time. In this case, the behavior of the cube starting from its entry in plasticity can be studied by not giving so much importance to the elastic regime that precedes it and that has already been several times described. In this case of plasticity, $\bar{\sigma} \geq \sigma_y$ and its definition can be first computed as:

$$\bar{\sigma} = \sigma_y^0 + (t - t^*)\left(\frac{\sigma_{\max} - \sigma_y^0}{t_m - t^*}\right) = \sigma_y^0 + A(t - t^*), \tag{90}$$

where $t^* = 1.8s$ is the time for which the plasticity starts and $t_m = 2.5s$ is the time at which the maximal load is applied for the first time. The constant coefficient is renamed A for simplicity. Putting Eq. 90 and 89 into Eq. 84 and imposing that the effective strain $\bar{\varepsilon}^{vp}$ at t^* is zero gives:

$$\dot{\bar{\varepsilon}}^{vp} + \frac{h}{\eta}\bar{\varepsilon}^{vp} = \frac{A(t - t^*)}{\eta} \Leftrightarrow \bar{\varepsilon}^{vp}(t - t^*) = \frac{A}{h}(t - t^*) + \frac{A\eta}{h^2}\left[exp\left(-\frac{h(t - t^*)}{\eta}\right) - 1\right], \ \forall t \in [t^*; t_m]. \tag{91}$$

This explains why $\bar{\varepsilon}^{vp}$ increases rapidly for t close to t^* but then, the effect of the exponential fades away and the increase is mostly linear. Then, the behavior of the strains when $\bar{\sigma} = \sigma_{\max}$ constant is simpler:

$$\dot{\bar{\varepsilon}}^{vp} + \frac{h}{\eta}\bar{\varepsilon}^{vp} = \frac{\sigma_{\max} - \sigma_y^0}{\eta} \Leftrightarrow \bar{\varepsilon}^{vp}(t - t^*) = Bexp\left(\frac{-h(t - t^*)}{\eta}\right) + \frac{\sigma_{\max}}{h} - \frac{\sigma_y^0}{h}, \tag{92}$$

where B is a constant that can be obtained while putting Eq. 92 into Eq. 89 and taking into account the fact that $\sigma_y(t^*) = \sigma_y^0$:

$$\bar{\varepsilon}^{vp}(t - t^*) = \left(\frac{\sigma_y^0 - \sigma_{\max}}{h}\right) exp\left(\frac{-h(t - t^*)}{\eta}\right) + \frac{\sigma_{\max}}{h} - \frac{\sigma_y^0}{h}. \tag{93}$$

This result explains the exponential behavior obtained in Fig. 49b. This phenomenon is not present for an elasto-plastic material, it is a particular behavior of the elasto-viscoplasticity called creep. It means that even if the stress is constant, the strain keeps increasing in time until it reaches a constant and asymptotic value (cf. Fig. 49b). In fact, when $t[s]$ increases, the exponential becomes negligible and $\bar{\varepsilon}^{vp} \to \frac{\sigma_{\max} - \sigma_y^0}{h} = 0.25\%$.

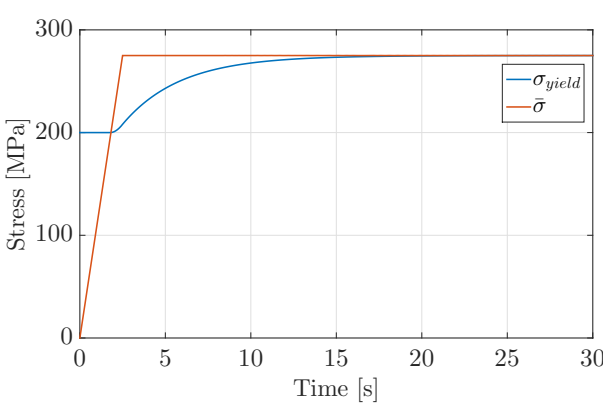

(a) Evolution in time of the stresses.

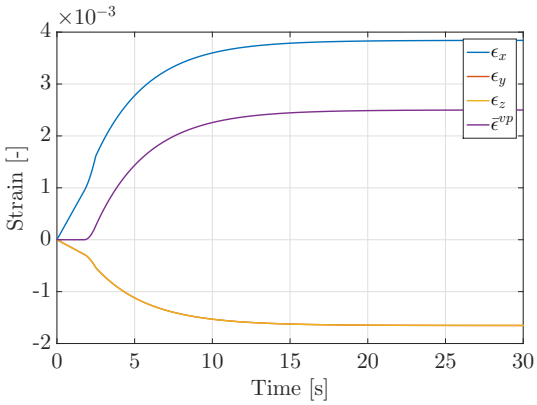

(b) Evolution in time of the strains.

Figure 49: Linear isotropic hardening model for $\eta = 10^5$ MPa.s for the imposed load kept constant at $t_{\max}$.

Thanks to Eq. 89 and Eq. 93, it is possible to compute the expression of the signed distance of the *Haigh Westergaard's space* once the load is constant ($t \geq t_m$):

$$\begin{aligned} d &= \bar{\sigma} - \sigma_y \\ &= \sigma_{\max} - \left[h \left(\left(\frac{\sigma_y^0 - \sigma_{\max}}{h} \right) \exp\left(\frac{-h(t-t^*)}{\eta} \right) + \frac{\sigma_{\max}}{h} - \frac{\sigma_y^0}{h} \right) + \sigma_y^0 \right] \\ &= (\sigma_{\max} - \sigma_y^0) \exp\left(\frac{-h(t-t^*)}{\eta} \right). \end{aligned} \tag{94}$$

This explains the behavior of the overstress shown in Fig. 50. It shows also that when time increases, the exponential becomes negligible so does the overstress. Therefore, for a long duration of time, σ_y tends to $\bar{\sigma}$ (cf. Fig. 49a). More physically, it can be interpreted by the fact that the yield surface expands always slower and slower until reaching the constant equivalent stress.
The influence of η can also be emphasized: if η increases, the curve of d will decrease less quickly until zero.

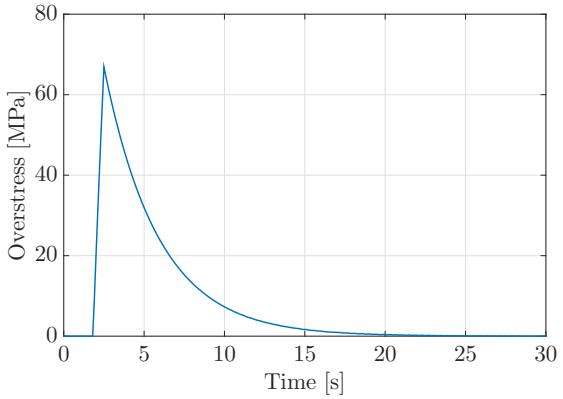

Figure 50: Evolution in time of the overstress for a linear isotropic hardening model, $\eta = 10^5$ MPa.s and the imposed load kept constant at $t_{\max}$.

If the preceding sawtooth loading, presented in Part 1, is modified by adding steps at the load extrema (cf. Fig. 51a), a similar analysis can be made. In order to understand the effect of this kind of loading on the equivalent visco-plastic strain, Fig. 52 and 51b may be analyzed step by step. The cube is first subjected to tension. While the load is smaller than the yield stress, $\bar{\varepsilon}^{vp}$ and σ_y are equal to zero. Then, at $0.9s$, the cube

enters in plasticity so the overstress d, $\bar{\varepsilon}^{vp}$ and σ_{yield} start to increase (the effective stress state is taken away from the yield surface). After $1.3s$, the load reaches its first plateau ($\sigma_x = t_{\max}$) during which $\bar{\varepsilon}^{vp}$ increases linearly. After $2.5s$, the cube is unloaded. The slope of $\bar{\varepsilon}^{vp}$ starts so to decrease until reaching zero. During this time, d is decreased until zero. Indeed, it is canceled when $\bar{\sigma}$ is lower than σ_y by its definition. The stress state is now back inside the yield surface. When the cube is completely unloaded, the load is kept null from $3.8s$ to $5s$ but the value of $\bar{\varepsilon}^{vp}$ stays constant until $5.9s$. This is because at $5s$, the cube is submitted to compression and, as it was the case in tension, it takes $0.9s$ to enter in plasticity. Finally, one can note that a peak appears in the overstress graph for each entry in plasticity. However, the maximum value of this one decreases at each time that the stress state goes out of the yield surface. It is because, every time the load reaches $t_{\max}$ or $-t_{\max}$, the value of $\bar{\sigma}$ has the same values while σ_y is always increased (until it reaches its asymptotic value). Indeed, at each loading, the material is hardened and the yield surface is a little bit more expanded. The amplitude of the peaks in the graph of d decreases until reaching zero for an infinitely long time because σ_y tends to $\bar{\sigma}$ as just explained.

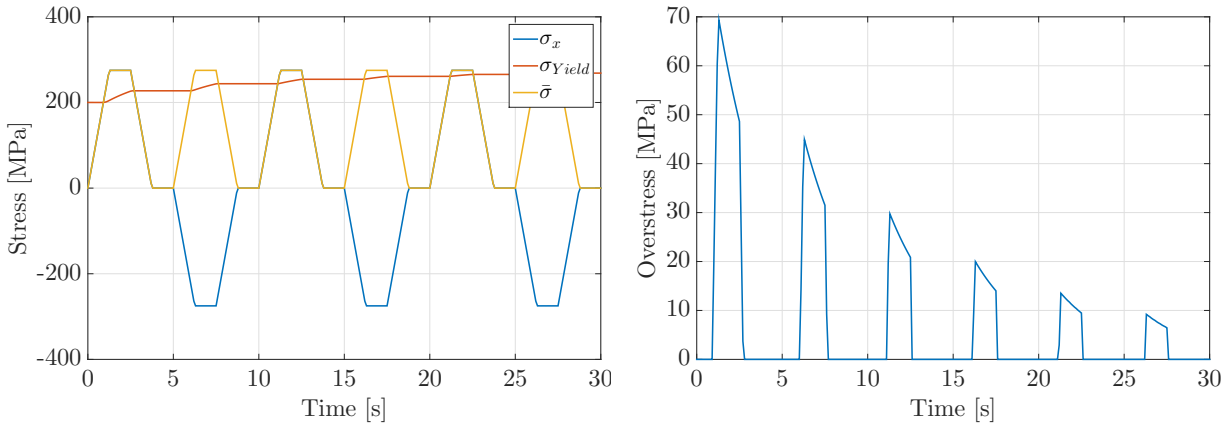

(a) Evolution in time of the stresses.

(b) Evolution in time of the overstress.

Figure 51: Linear isotropic hardening model for $\eta = 10^5[MPa.s]$ for a cycling loading with the imposed load kept constant at $t_{\max}$, 0 and $-t_{\max}$.

By way of comparison, the two different strains obtained for both types of loading have been superimposed in Fig. 52. It can be concluded that the equivalent strain is larger in the case of the loading with plateaus. This result was expected since when $\sigma_{11} = \pm t_{\max}$, the load is kept constant. And during this duration of time, the stress state is outside the yield surface. It thus means that $\bar{\varepsilon}^{vp}$ is increased during a longer time than in the simple sawtooth case. It is why the orange curve is higher than the blue one. As it increases faster, $\bar{\varepsilon}^{vp}$ reaches sooner its asymptotic value (as explained in Part 1).

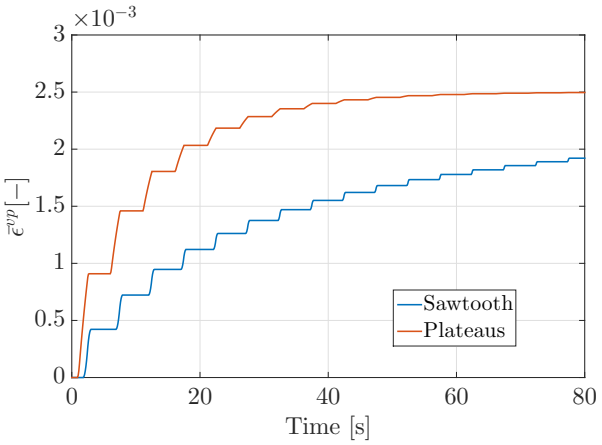

Figure 52: Evolution in time of the strain with a linear isotropic hardening model for $\eta = 10^5$ MPa.s for a cycling loading with the imposed load kept constant at $t_{\max}$, 0 and $-t_{\max}$.

8.3 Mixed hardening model

To illustrate this model, the same loading as the one used for the linear isotropic case has been applied; it means that the maximal load $t_{\max}$ is applied for an infinitely long time. Now, note that the hardening coefficient becomes $h = h_i + h_k$ and a backstress $\boldsymbol{\alpha}$ is added. Thus, it is important to note that the expression of the yield stress has changed. Indeed, it is now expressed as:

$$\sigma_y = h_i \bar{\varepsilon}^{vp} + \sigma_y^0. \tag{95}$$

This is the reason why σ_{yield} (cf. Fig. 53a) increases less rapidly than in Fig. 49a: $h_i = (\theta^* \times h) < h$ here. However, the shapes are really similar. In Fig. 53b, one can see that $\bar{\varepsilon}^{vp}$ adopts also the same behavior as in the isotropic model described here above. Therefore, these behaviors will not be further detailed.

The evolution of $\dot{\boldsymbol{\alpha}}$ is given by Eq. 86. It is directly proportional to the normal tensor $\boldsymbol{N}$. In a plane stress state, this tensor always keeps a constant value at the point where the stress tensor is applied on the surface. Therefore, the only remaining variable in the evolution of the backstress is the overstress d (cf. Fig. 54b) which takes the same expression as the one presented in Eq. 94 (for $h = h_i$). The behavior of $\bar{\alpha}$ (cf. Fig. 54a) can be deduced from this. Indeed, $\bar{\alpha}$ begins to increase at the entry in plasticity with a slope that decreases more and more (exponential behavior) until it reaches a constant value when $d = 0MPa$. In fact, $\dot{\bar{\alpha}}$ will tend to zero too for an infinitely long time.

One can notice that the evolution of $\bar{\sigma}^{VM}$ is also different from the isotropic model. Indeed, since there is now a backstress that increases with time once in plasticity, by its definition, $\bar{\sigma}^{VM}$ will first be slowed down. After that $t_{\max}$ is reached, $\bar{\sigma}^{VM}$ decreases continuously due to the further increase of the absolute value of the components of α_{ij}. Since the overstress is the difference between $\bar{\sigma}^{VM}$ and σ_{yield}, its plot is consistent (cf. Fig 54b). When the load is higher than σ_y^0, the overstress rapidly increases but starts to decrease as soon as $\bar{\sigma}^{VM}$ starts to drop.

It can be concluded that the results are very similar to the case of the linear isotropic hardening. The difference is mainly due to the presence of a backstress but this does not lead to huge dissimilarities between the two behaviors.

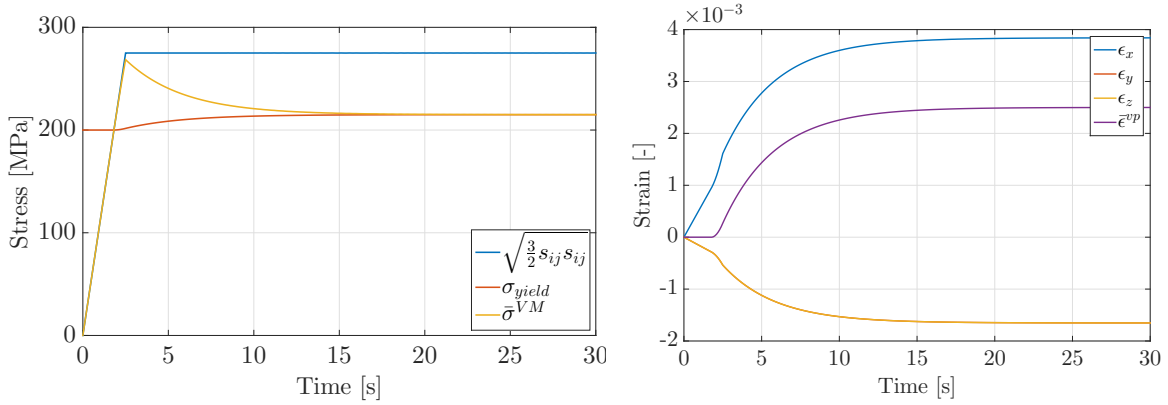

(a) Evolution in time of the stresses.

(b) Evolution in time of the strains.

Figure 53: Linear mixed hardening model for $\eta = 10^5$ MPa.s for the imposed load kept constant at $t_{\max}$.

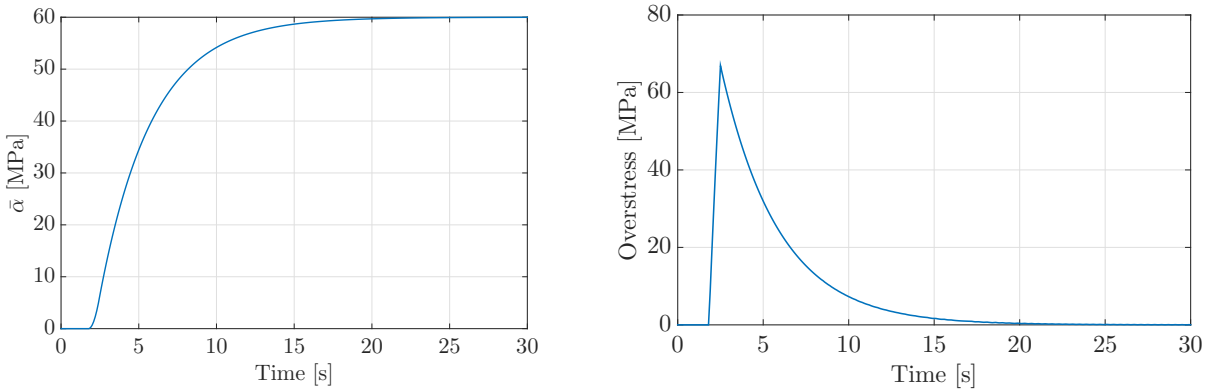

(a) Evolution in time of the backstress.

(b) Evolution in time of the overstress.

Figure 54: Linear mixed hardening model for $\eta = 10^5$ MPa.s for the imposed load kept constant at $t_{\max}$.

The results obtained when a cycling loading is applied as depicted in Fig. 55a are similar to those obtained with the same loading in the linear isotropic case. Indeed, as the material enters several times in plasticity, $\bar{\varepsilon}^{vp}$ increases by steps (cf. Fig. 55b). One can notice that once again, the plateaus allows to stay longer in plasticity and thus to reach sooner the asymptotic value.

Nevertheless, there are some differences between the two models. Firstly, the presence of the backstress modifies the evolution of $\bar{\sigma}^{VM}$ because it is not simply equal to $\sqrt{\frac{3}{2}s_{ij}s_{ij}}$ anymore as just mentioned. Indeed, during all the plasticity, $\bar{\alpha}$ has a non-zero slope (cf. Fig. 55c). This explains the shattered peaks in Fig. 55a for $\bar{\sigma}^{VM}$.

Another important difference is the evolution of the overstress (cf. Fig. 55d). Indeed, it first rapidly evolves when the load becomes higher than the yield stress then it slowly

decreases when σ_{11} reaches a plateau at $t_{\max}$ and $-t_{\max}$ (due to the evolution of $\bar{\sigma}^{VM}$ just described). The overstress then drops and comes back to zero when the stress is brought back to the yield surface.

At the beginning, the maximum amplitude of the peaks does not decrease as fast as in the isotropic model. Indeed, even if σ_{yield} increases (and thus the yield surface expands) with plasticity, the maximum value of $\bar{\sigma}^{VM}$ increases also in time due to the large decrease of α during the first compression. Nevertheless, as described in Part I, the duration spent in plasticity will decrease with time, so that the difference between $\bar{\alpha}$ in traction and compression will tend to zero and the amplitude of the overstress peaks will decrease as well. It is explained by the fact that the yield surface is not only expanded but also translated at each entry in plasticity until reaching an asymptotic value.

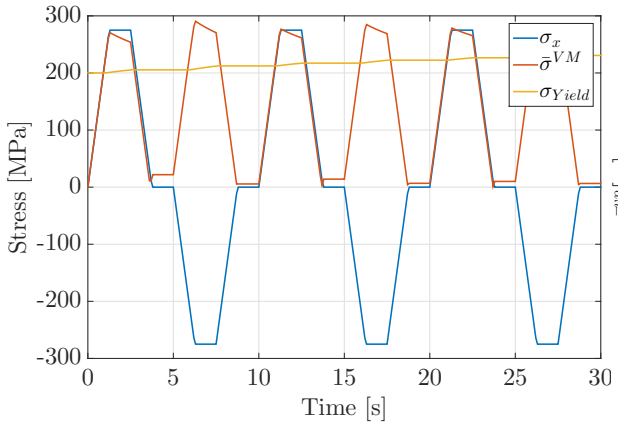

(a) Evolution in time of the stress.

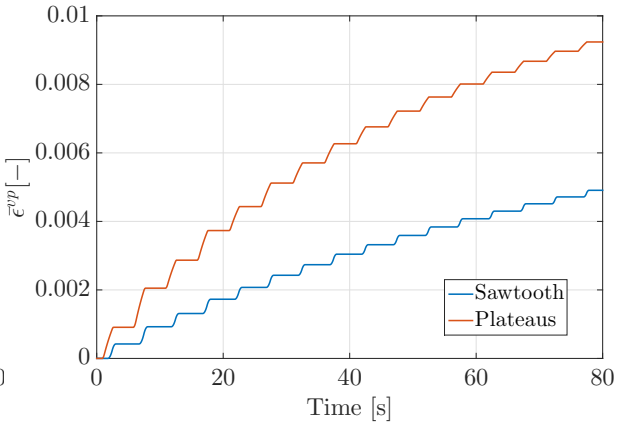

(b) Evolution in time of the strain.

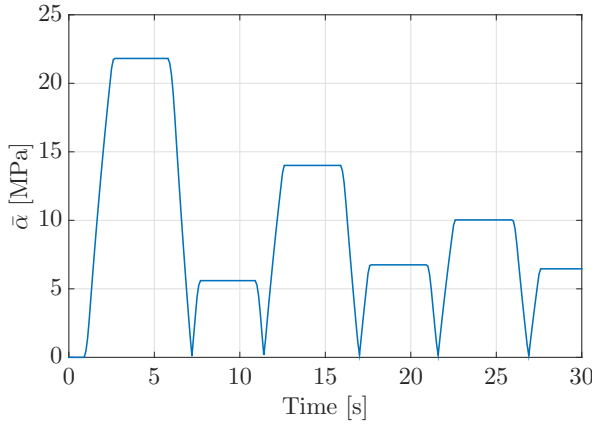

(c) Evolution in time of the backstress.

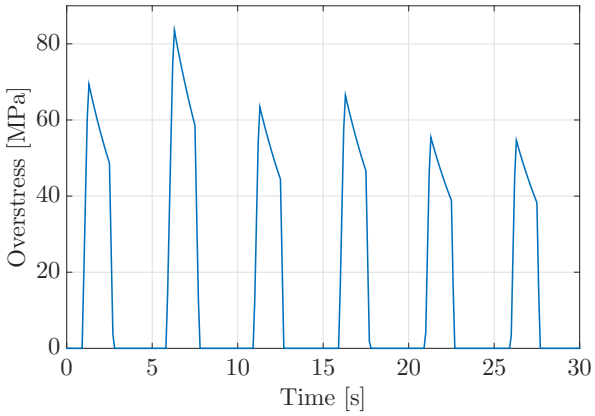

(d) Evolution in time of the overstress.

Figure 55: Linear mixed hardening model for $\eta = 10^5$ MPa.s for a cycling loading with the imposed load kept constant at $t_{\max}$, 0 and $-t_{\max}$.

Part IV
Sensitivity study of numerical parameters

In this part, numerical parameters such as the loading speed, the spatial discretization, and the temporal discretization will be studied through their effects on the numerical simulations.

9 Principle of virtual work

To solve a 3D plastic problem, there is no analytical solution; therefore, a finite element method is used. This method is base on the weak form of the principle of virtual work. It consists in imposing a continuous virtual displacement δu_i where displacements are not imposed by the boundaries.

Since the virtual work done by the inertia forces is neglected here, a quasi-static case is considered as already mentioned. Therefore, the principle of virtual work writes as follow:

$$\delta W_{int} = \delta W_{ext}, \tag{96}$$

where

$$W_{int} = \int_0^{t_f} (\vec{F}^{int}(t).\dot{\vec{q}}(t))dt \quad \text{and} \quad W_{ext} = \int_0^{t_f} (\vec{F}^{ext}(t).\dot{\vec{q}}(t))dt. \tag{97}$$

with $\dot{\vec{q}}(t)$ the structural nodal velocity vector. The equilibrium must be checked at each increment. To do so, the following equation must be satisfied:

$$\underbrace{\vec{F}^{OOB}(t)}_{\text{Out of balance forces}} = \vec{F}^{int}(t) - \vec{F}^{ext}(t) = \vec{0}. \tag{98}$$

If this equation is not verified at the predictor phase, supplementary iterations have to be made using a corrector phase until this equality is respected. This is the principle of Newton-Raphson algorithm implemented in Metafor.

However, one can notice that these out of balance forces will almost never be exactly equal to 0 for each degree of freedom. That is why a tolerance is defined as follow:

$$\frac{\|\vec{F}^{OOB}\|}{\|\vec{F}^{ext}\|} < \epsilon. \tag{99}$$

where the tolerance ϵ is about 10^{-4} in Metafor. Finally, it can be added that the work carried out by the internal and external forces in a purely elastic case will take a null value. Indeed, there is no dissipation due to plasticity and all the processes are reversible ones.

10 Influence of loading speed and temporal discretization

Both the influence of the loading speed and of the temporal discretization will be investigated together. Indeed, they are closely related since the loading speed depends strongly on the duration of the period and on the time step.

One thing essential to know is the fact that the value of the maximum time step is imposed in the python code and that the software can adjust this Δt to ensure the convergence of the solution. Indeed, if the number of iterations needed to reach a residual smaller than the tolerance is smaller than three, the time step is increased and if it is greater than four, it is refined. Nevertheless, it does not guarantee the precision of the results as it will be shown below.

10.1 Elasto-plastic model

In this section, the linear hardening models are first considered and are then extended to the non-linear cases.

There are different things that influence the accuracy of the results in a linear hardening model. Firstly, the quarter of the period must be an integer multiple of the time step in order to properly capture the specific times at which $\sigma_{11} = t_{max}, 0$ and $-t_{max}$ that are the peaks of the loading cycle. Indeed, if the time steps can not intercept the maxima and the transition from traction to compression, the sharp corners become shattered ones as those presented in Fig. 56a for σ_{11} at the quarter of the period or for a $\bar{\sigma}^{VM}$ close to zero.

In the same idea, the entry in plasticity is an important point that must be captured by the software. Otherwise, the cube will pass from the elastic regime to the plastic one without identifying the real transition point for which the yield stress is reached. This phenomenon is represented in Fig. 56b: the effective plastic strain should behave as shown in Fig. 8b; however, the change in slope due to the entry in plasticity is carried out in two stages.

These two constraints imposed on the time step can be rewritten as following, where a and b must be integers that represent respectively the number of time steps needed to reach the quarter of the period and to enter for the first time in plasticity:

$$\begin{cases} \frac{T}{4} = a\Delta t \\ \frac{\sigma_y^0}{b\Delta t} = \frac{\sigma_{max}}{\frac{T}{4}} \end{cases} \tag{100}$$

Additionally, an other important thing must be verified in order to obtain meaningful results. While applying the load, it will be decomposed into a number of sub-increments (equal to the number of time steps). If this number is too small, the equilibrium configuration is not reached and the Newton-Raphson process does not converge. This is due to the loading speed which is too high as shown in Fig. 57. Theoretically, the maximal load should be applied through 10 time steps and therefore, the period should be equals to 40 times the time step in the ideal case (for the sawtooth path). However, one can

remark that only five time steps seem to be already sufficient to interpret the results.

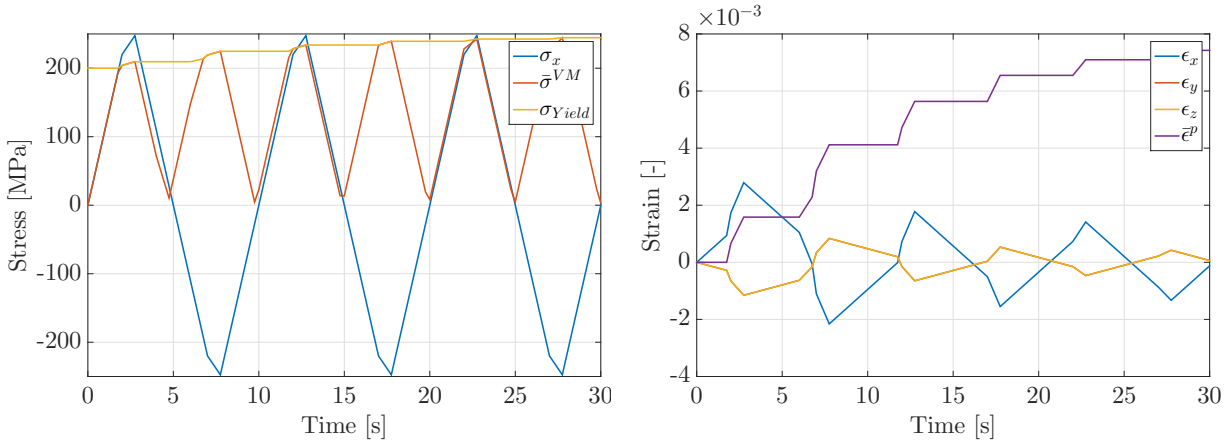

(a) Evolution in time of the stresses.

(b) Evolution in time of the strains.

Figure 56: Linear mixed hardening with a time step of 0.5s and a period of 10s.

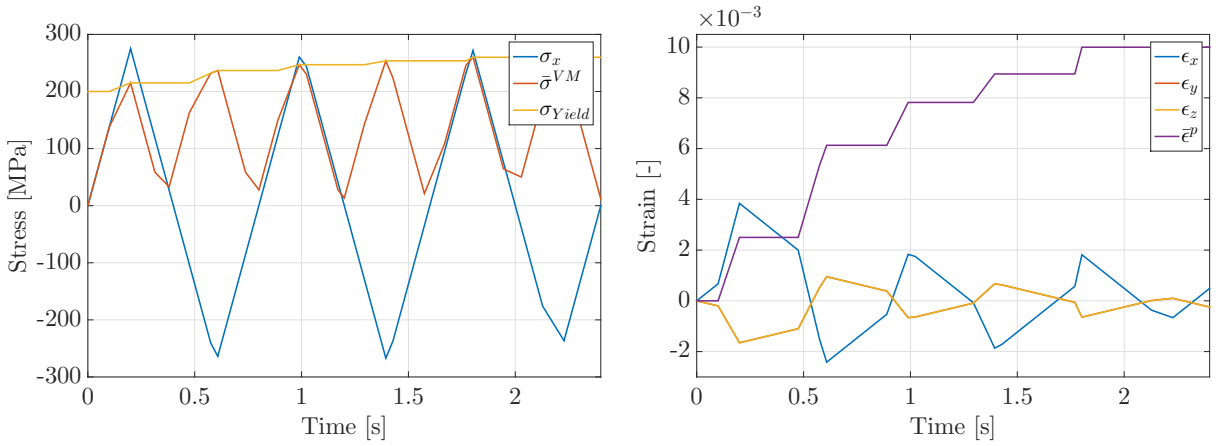

(a) Evolution in time of the stresses.

(b) Evolution in time of the strains.

Figure 57: Linear mixed hardening with a time step of 0.1s and a period of 0.4s.

As a summary, one can say that the elasto-plastic model is numerically dependent on the loading speed, which is not the case from a physical point of view since the simulation requires some specific constraints in order to converge.

10.2 Elasto-viscoplastic model

As it has been said in Part III, with an elasto-viscoplastic model, the behavior of the material is strongly dependent on the loading speed. Thus, the study cannot only consider this parameter as it has been done in the previous section. Hereafter, only the time step will be modified and the consequences of this change will be studied.

In the previous section, it has been shown that, to be able to catch correctly the extrema of the loading cycle, the quarter of the period of the applied load should be an integer multiple of the time step. Moreover, the load has to be applied in minimum 5

times steps to obtain converged results. With elasto-viscoplastic materials, the conditions presented here above are not sufficient anymore to have accurate results.

In fact, in this case, the smaller the time step, the more precise the results. In Fig. 58, the strains obtained with a linear mixed hardening model have been plotted for an elasto-viscoplastic material for different time steps and for a period $T = 10s$. The first time step has been taken equal to $0.75s$ such that the quarter period is a multiple of it. The second has been chosen as a reference because it is much smaller and thus gives more accurate curves. Indeed, one can note that the difference between the curves obtained with the two time steps (the full line compared to the dashed one) is quiet large.

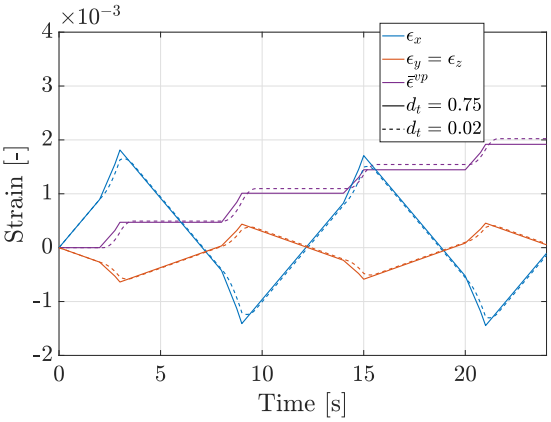

Figure 58: Influence of the time step with a linear mixed hardening model for an elasto-viscoplastic material with a period $T = 12s$.

To conclude, even if the best suited numerical parameters are the same for elasto-plastic material with a linear and a non-linear hardening model, they do not give accurate results for an elasto-viscoplastic material with hardening.

11 Influence of spatial discretization

The spatial discretization can be done by the finite element method. It consists in dividing geometrically the solid studied in order to obtain a finite number of elements and easily get an approximation of the displacements. The idea is to compute the equations only at the nodes of the finite element mesh.

Usually, the finer the mesh, the more accurate the results. But in the study of this report, it is not the case. Indeed, the cube is only submitted to a uni-axial surface traction so the strains and the stresses are uniform inside the cube.

Moreover, the displacements computed during this project are only considered at one point of the cube (one of its corner) so the number of mesh elements does not matter.

Conclusion

The aim of the current study was to analyze the behavior of a cube subjected to a uniform traction, in particular when this loading introduces plasticity.

Firstly, an elasto-plastic behavior has been assumed for the material. In the plane stress case, different linear hardening models have been compared: perfectly plastic, isotropic, kinematic and mixed hardening.

For a perfectly plastic model, it has been shown that the material presents a purely elastic behavior when the load is lower than the virgin yield stress but once it is reached, the material deforms without any increase in the applied stress but it cannot be represented using the Metafor numerical scheme.

For a linear isotropic model, a maximum surface traction needed during the first loading cycle to reach a permanent equivalent viscoplastic deformation has been determined. It has been shown that since the applied load will never be larger than t_{max}, the material will never harden anymore. Therefore, after one cycle, the yield surface has expanded for good and all the processes of loading/unloading are purely elastic.

Then, it has been presented that for a linear kinematic model, the yield surface is just translated. Another difference is that the equivalent plastic strain does not reach a constant value but is increased at each entry in plasticity.

Finally, it has been concluded that the linear mixed hardening model was the more realistic one. Here, the yield surface is expanded and translated at each loading/unloading cycle due to the combined effects of the isotropic and kinematic models, respectively. It finally reaches an asymptotic value after an infinite number of cycles.

The same analyses have been proceeded in a plane strain state. It has been demonstrated that for each model, the conclusions were quiet the same than in the configuration of plane stress. The main difference was that because of the additional boundary conditions, additive stresses were born inside the material and so more complex phenomena may be observed.

A global discussion has then be led. The analyze of the plastic dissipation has shown that with the kinematic model the plastic dissipation tends to infinity while the isotropic and mixed ones tend to a finite constant value.

In the second part of the project, the material was still assumed to have an elasto-plastic behavior but the models used to describe hardening were non-linear ones. To describe kinematic hardening, the non-linear *Armstrong Frederick's* evolution law of the backstress tensor has been used. This ones takes into account a restoring force that tends to bring back the center of the yield surface to its initial position. The influence of this force has been studied through the dynamic recovery parameter η_k and its limit values have been determined. It has also been shown that, depending on the current position of the center of the yield surface and on the direction of the loading, the recovery force acts either in favor or against the driving effect.

Furthermore, the *Haigh Westergaard's space* has been used to graphically study the influence of the non-linear recovery term : it has been figured out that the plastic modulus

H^p which is the slope of the curve $\bar{\sigma} - \bar{\varepsilon}^p$ was always decreasing during plasticity.

Finally, the behavior of the cube has been studied for different values of the prescribed loading $t_{\max}$ and for different combination of the hardening models: the *Armstrong Frederick's* model was first studied in purely kinematic hardening, then combined with linear isotropic hardening, and at the end combined with non-linear isotropic hardening described by *Voce's* saturated law.

For the purely kinematic case the yield stress remains the one of the virgin material. The plasticity results only in a translation of the yield surface. This translation is limited: at some point, the recovery force becomes so high that it cancels out the driving force and the backstress does not evolve anymore. An asymptotic yield surface can be defined since the equivalent stress is bounded by the sum of this asymptotic backstress and the yield stress. A comparison between the linear kinematic hardening model and the non-linear one in terms of plastic dissipation has also be performed. This showed that the plastic dissipation in the case of a non-linear kinematic hardening was bigger than in the case of a linear kinematic hardening.

For the combination of non-linear kinematic hardening with linear isotropic hardening, it has been pointed out that the equivalent stress $\sqrt{3J_2}$ was not bounded since the yield stress can in theory increase infinitely with the applied load t_{max}. This leads to the fact that the yield surface will expand. It will be expanded so much that all the processes of loading/unloading will take place in elasticity. That is why the equivalent plastic strain tends to an asymptotic value, and the backstress tends to a zero value across the cycles.

In the last combination of non-linear kinematic hardening with linear isotropic hardening, the limit value for the yield stress has been high-lighted. Due to this asymptotic value, the yield surface is limited in its expansion, and this leads to the fact that the equivalent stress $\sqrt{3J_2}$ is thus bounded in contrary to the previous combination, the asymptotic yield surface has therefore be defined. Two different cases have been analyzed. If the applied load is between the initial yield stress and the asymptotic one, plasticity occurs in several cycles before being reduced by the increase of the yield stress. Therefore, the equivalent plastic strain stabilizes and the backstress tends to zero. Reversely, when the applied load is higher than σ_y^∞, plasticity will continue after that the yield stress reaches its asymptotic value, with a purely kinematic behavior.

In the third part of this project, an elasto-viscoplastic material has been studied thanks to the introduction of η with three models: one without any hardening, a linear isotropic one and a linear kinematic one. It turned out that the higher the η, the lower the strain rate. Then, different kinds of loading have been tested: the simple sawtooth cycle presented in the introduction, the same one but with the load kept constant during some time when it reaches $t_{\max}$, $-t_{\max}$ and 0 and finally, a loading keeping the stress constant at the maximum value t_{max}. These different applied forces have allowed to observe that this kind of material is really time dependent, its behaviors depending on the loading rate. The main difference with an elasto-plastic material is that, when viscosity is considered, the stress state can go out of the yield surface. Another parameter has thus been introduced: the overstress d. It allows to characterize the distance between the stress state and the yield surface.

In the fourth and last part, the influence of numerical parameters such as the loading speed, the temporal discretization and the spatial discretization have been investigated.

In order to have accurate results for the *Newton-Raphson* algorithm, the ratio $\frac{\|\vec{F}^{OOB}\|}{\|\vec{F}^{ext}\|}$ has to be smaller than the tolerance of about 10^{-4}. This corresponds to the application of the principle of virtual work.

Then, the effects of the loading speed and the time step have been analyzed together since these two notions are coupled. For the elasto-plastic models, a particular attention has been accorded to the fact that the quarter-period should be at least equal to five times the time step in order to properly capture the extreme values of σ at their proper times and to apply the load with a low loading speed in order to ensure the convergence. A particular attention should also be added to properly capture the entries in plasticity.

For an elasto-viscoplastic material, since it is very sensitive to the loading rate, the study of this parameter in this case has not been made. However, it has been concluded that the smaller is the time step, the better the results.

Finally, it was concluded that the study of the spatial discretization is not consistent in this case since the cube is subjected to a uniform loading and the displacements are considered at only one of the cube corners.

Bibliography

[1] J.-P. Ponthot. Advanced Solid Mechanics. Lectures notes. Version 2020-2021.

[2] J.-P. Ponthot. Finite Element Method. Lectures notes. Version 2019-2020.